

Strategies to Improve the Output Performance of Triboelectric Nanogenerators

Cong Li, Yuan Bai, Jiajia Shao, Hongyu Meng,* and Zhou Li*

Triboelectric nanogenerators (TENGs) can collect and convert random mechanical energy into electric energy, with remarkable advantages including broadly available materials, straightforward preparation, and multiple applications. Over the years, researchers have made substantial advancements in the theoretical and practical aspects of TENG. Nevertheless, the pivotal challenge in realizing full applications of TENG lies in ensuring that the generated output meets the specific application requirements. Consequently, substantial research is dedicated to exploring methods and mechanisms for enhancing the output performance of TENG devices. This review aims to comprehensively examine the influencing factors and corresponding improvement strategies of the output performance based on the contact electrification mechanism and operational principles that underlie TENG technology. This review primarily delves into five key areas of improvement: materials selection, surface modification, component adjustments, structural optimization, and electrode enhancements. These aspects are crucial in tailoring TENG devices to meet the desired performance metrics for various applications.

electrostatic induction,^[3–5] allowing it to tap into a diverse range of mechanical energy sources that typically go untapped in daily life, such as wind energy,^[6–8] water waves,^[9–11] and physiological processes like heartbeats,^[12,13] breathing,^[14–16] and so on.^[17–23] The inception of TENG has sparked a global surge in research across various energy-related domains. TENG boasts distinct advantages over established technologies, including its compact size, lightweight design, cost-effectiveness, straightforward fabrication, and the wide array of materials at its disposal.^[24–27] When constructed with suitable materials and well-designed structures, TENGs can seamlessly integrate into self-driven systems, offering a sustainable power source for electronic devices.^[28] This heightened research interest has led to the expansion of TENG's application possibilities, ranging from blue ocean

energy harvesting^[29–31] to wearable, flexible sensors,^[32–38] biomimetic and smart devices,^[39–42] as well as self-powered implantable and micro medical devices.^[34,35,37,43–46]

As an energy harvester, TENGs are often expected to achieve higher energy conversion efficiency, directly correlating with improved output performance. Moreover, TENG-based sensors exhibiting superior output performance offer increased sensitivity and signal-to-noise ratio, making it essential to enhance the output performance of TENG devices for a wide range of practical applications.^[47,48] Studies have shown that the maximum surface charge density (MSCD) of triboelectric materials plays a pivotal role in influencing the average output power and energy conversion efficiency of TENG. MSCD essentially determines the output level, making it an effective approach to enhance charge generation during the friction process.^[49–51] Alongside MSCD, several other influencing factors come into play, such as material properties,^[24,52–54] the contact area of triboelectric layers,^[49,55,56] device configuration,^[57,58] and environmental conditions, encompassing aspects like temperature,^[59,60] humidity,^[61,62] external mechanical states,^[63,64] electric field,^[65,66] and magnetic field.^[67,68]

Researchers have made significant strides in enhancing the output performance of TENG by addressing various aspects. These methods encompass material selection,^[24,52] surface modification,^[69,70] composition of different components,^[71,72] device structure design,^[57,73] electrode optimization,^[74,75] and

1. Introduction

In 2012, Zhong Lin Wang et al. introduced the concept of the triboelectric nanogenerator (TENG), a novel technology designed for capturing and harnessing ambient mechanical energy.^[1,2] TENG leverages the combined effects of triboelectrification and

C. Li, Y. Bai, J. Shao, H. Meng, Z. Li
Beijing Institute of Nanoenergy and Nanosystems
Chinese Academy of Sciences
Beijing 101400, China
E-mail: menghy@iccas.ac.cn; zli@binn.cas.cn

C. Li
School of Chemistry and Chemical Engineering
Guangxi University
Nanning, Guangxi 530004, China

Y. Bai, Z. Li
Center on Nanoenergy Research, School of Physical Science and Technology
Guangxi University
Nanning 530004, China

J. Shao, Z. Li
School of Nanoscience and Technology
University of Chinese Academy of Sciences
Beijing 100049, China

 The ORCID identification number(s) for the author(s) of this article can be found under <https://doi.org/10.1002/smtd.202301682>

DOI: 10.1002/smtd.202301682

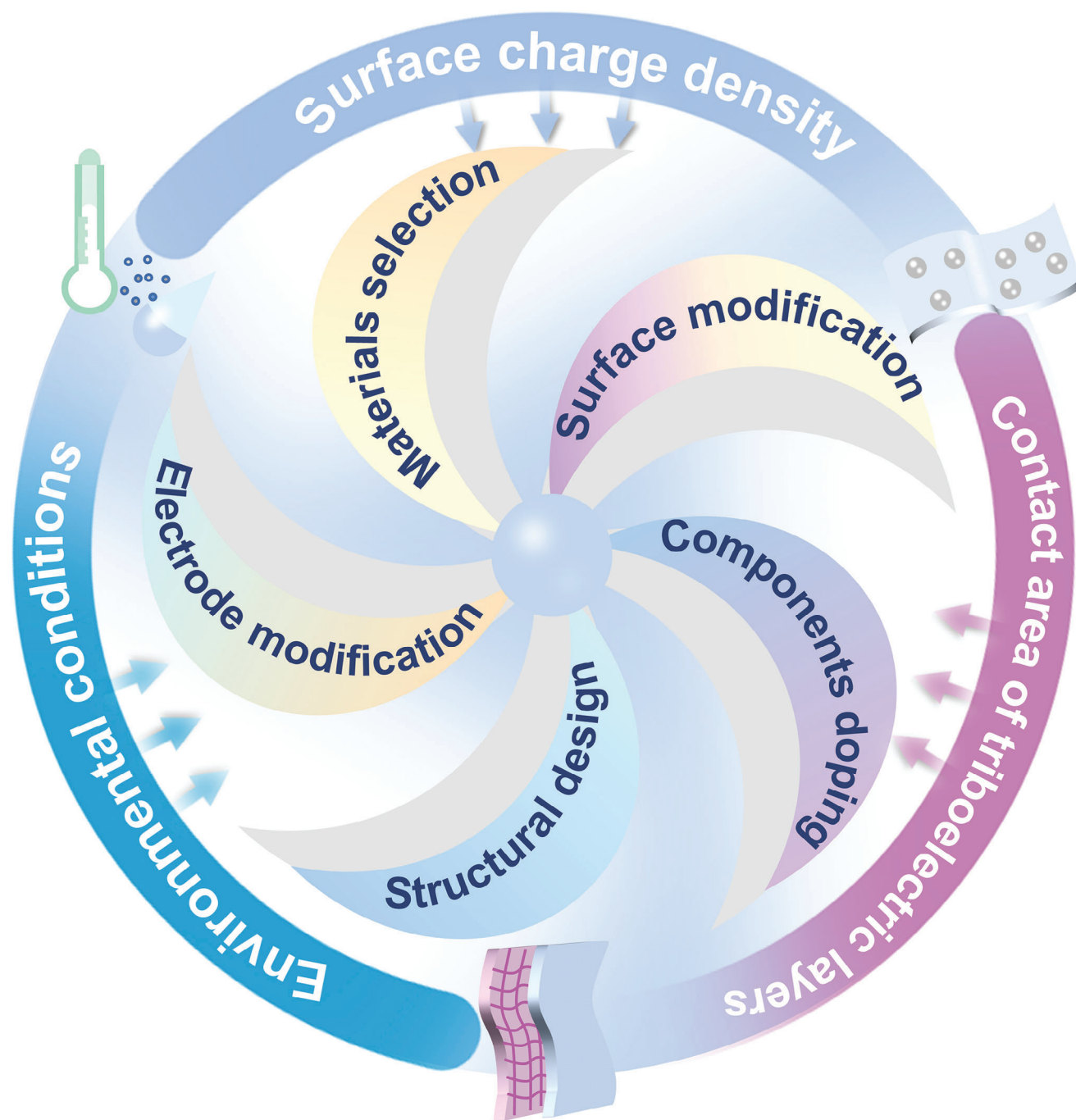


Figure 1. Schematic overview of the influencing factors and improvement methods of the output performance of TENG devices.

regulation of environmental conditions.^[76,77] The selection of appropriate materials relies on the triboelectric series as a fundamental criterion. Surface modification and component doping are valuable techniques for altering the electron-donating (ED) and electron-withdrawing (EW) capabilities of materials, leveraging both physical and chemical methods. The strategic design of TENG device structures leads to a substantial improvement in output power, enabling their adaptability to a broader range of application scenar-

ios. Moreover, electrode modification methods merit consideration, including material selection and structural design of electrodes.

This review analyzes influencing factors and introduces improvement methods for the output performance of TENG from five aspects (**Figure 1**). Finally, it highlights the challenges to overcome. It also outlines the future improvement direction of TENG, aiming to guide the development of TENG with higher output and extensive application.

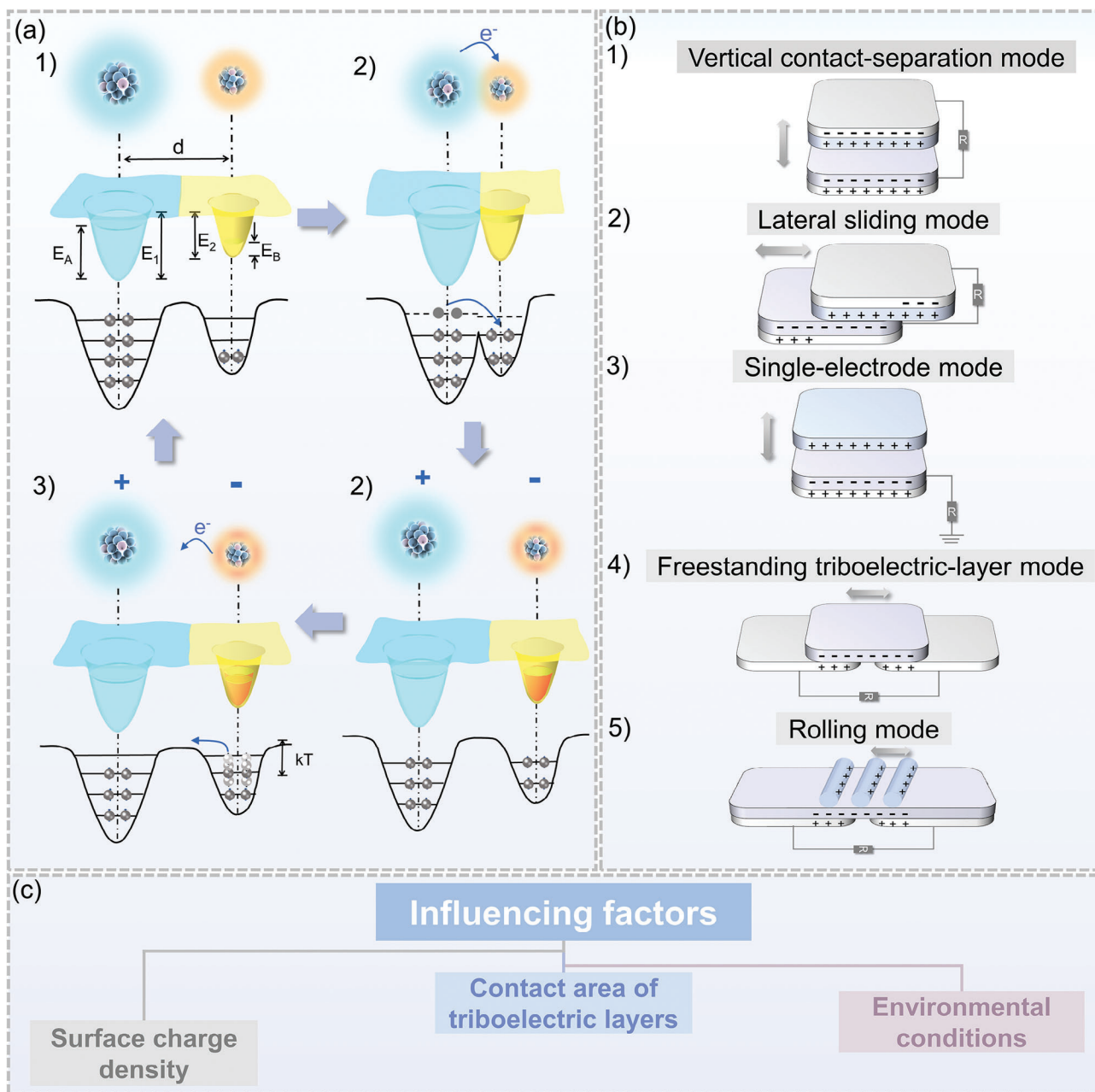


Figure 2. The mechanism of the TENG. a) An electron-cloud-potential-well model is proposed to explain contact-electrification (CE) mechanism, charge transfer, and release between two materials when they are 1) before contact, 2) in contact, and 3) after contact. b) The five operating modes are 1) vertical contact-separation (CS) mode, 2) lateral sliding (LS) mode, 3) single-electrode (SE) mode, 4) freestanding triboelectric-layer (FT) mode, and 5) rolling (R) mode. c) Three main influencing factors of the output performance.

2. Working Mechanism and Influencing Factors

Contact-electrification (CE) is a universal effect primarily driven by the transfer of electrons between solid-solid pairs. This effect finds its basis in an atomic-level charge transfer mechanism, as initially proposed by Wang.^[78] Before the atomic-level contact between the two materials, their respective electron clouds remained separate and non-overlapping. Within this state, electrons are tightly bound in specific orbitals by potential wells, making their escape challenging (as depicted in Figure 2a(1)). When

the atoms of these two materials come into close contact, their electron clouds start to overlap, resulting in the formation of ionic or covalent bonds. The bonding lengths further decrease if an external compression force is applied. Consequently, the initial single potential wells evolve into an asymmetric double-well potential, with the increased overlapping strength reducing the energy barrier between them (as illustrated in Figure 2a(2)). This reduction in the energy barrier enables electrons to transfer from one atom to another, thereby giving rise to CE. After their separation (as shown in Figure 2a(3)), these transferred electrons

remain static charges on the material's surface. This fundamental CE mechanism serves as the cornerstone for the realization of TENG. Based on their device structure and operating mode, TENGs can be categorized into five fundamental types, specifically the vertical contact-separation (CS) mode,^[1,79] lateral sliding (LS) mode,^[64,80] single-electrode (SE) mode,^[81,82] freestanding triboelectric-layer (FT) mode^[17,83] and rolling (R) mode,^[84,85] as elucidated in Figure 2b(1–5)).

The output performance of TENG devices, often referred to as load characteristics, is a key indicator encompassing the open-circuit voltage (V_{oc}), short-circuit current (I_{sc}), and power density under specific operation conditions.^[86] Ensuring the device can generate the requisite power is crucial to meet its energy supply needs. In the context of CS-TENG, Wang et al. derived the relationship between the transfer charge Q , voltage V , and the distance x between the two electrodes.^[87] The equation is expressed as follows:

$$V = -\frac{Q}{S\epsilon_0}(d_0 + x(t)) + \frac{\sigma x(t)}{\epsilon_0} \quad (1)$$

where $x(t)$ is the separation distance between the two triboelectric layers, σ is the transfer charge per unit area, ϵ_0 is the vacuum permittivity, and d_0 is the effective permittivity.

This equation indicates that the output performance of TENG is directly proportional to the contact area S and the charge density σ of triboelectric layers. This means that the output performance of TENG can be improved by increasing the contact area and charge density on the triboelectric layer's surface.

In addition, external environmental conditions during operation will also noticeably impact the output performance of TENG (Figure 2c).

2.1. Surface Charge Density

The parameter that represents the density of charge distribution is known as surface charge density (SCD). An increase in the transferred charges per unit area indicates an elevation in the SCD of the triboelectric layer, resulting in a larger potential difference between the two poles, which in turn generates higher output performance. However, there is a limitation to SCD due to the restriction of air breakdown in practical environments.^[49,88,89] Although a vacuum environment can effectively avoid the air breakdown effect and improve the charge density to $1003 \mu\text{C m}^{-2}$,^[49] creating such a vacuum environment is technically complex and costly. Therefore, it is more worthwhile to consider optimizing the output by changing material properties and reducing charge loss. Specifically, triboelectric polarity, which refers to the ability to absorb or lose electrons, is a primary principle in selecting the triboelectric pair with a large polarity difference. The electrical conductivity is also essential because low electrical conductivity is often accompanied by high electric resistance, thus blocking the dispersion of charges in the material.^[90] Therefore, more transformed charges can accumulate on the material surface, and a strong potential difference is produced, achieving a high output power. So far, the highest triboelectric charge density (TECD) achieved by TENG operating in an air environment has reached 660 mC m^{-2} .^[91]

2.2. Contact Area of Triboelectric Layers

Charge transfer occurs in effective contact between the two triboelectric layer materials, and its efficiency is enhanced with the increase in the degree of contact. While increasing the size of triboelectric layers is intuitive and straightforward, researchers are more inclined to adopt modification techniques to alter the surface morphology of materials. In addition, the rough material surface with a larger specific surface area can remarkably increase the charge density being transferred during contact separation, thereby producing a higher output than the smooth surface. Furthermore, studies have proved that enhancing the surface roughness of triboelectric layers can increase the capacitances, thereby improving the charge-storing abilities.^[92] Appropriate surface roughness enhancement for materials by altering microstructures or introducing patterns can imbue the TENG device with lightweight, compact, and portability attributes. Under a small external force, both the contact area and output increase with the rise in force. However, the contact area reaches saturation under high external force, and the TECD also saturates.^[93] Therefore, adding micro/nanostructures on the surface of triboelectric layers can further promote charge transfer under high forces to a certain extent, thereby enabling the device to exhibit high-level outputs.

2.3. Other Influencing Factors

In addition to the two points mentioned above, the external load resistances directly affect the output performances because of the correlated relationship between the resistance and power density of TENGs.^[94] Besides, the output performance shows a dependence on the vibration frequency and driving force.^[63,64] Moreover, external environmental conditions significantly impact TENG output. These conditions encompass factors like temperature, humidity, electric field, and magnetic field, all necessitating regulation and control. Generally, high temperatures have an adverse effect on the storage and dissipation of electrons, leading to a significant decrease in output performance.^[59] Furthermore, environmental humidity harms the device as water molecules in the atmosphere can attach to the triboelectric surface, causing charge dissipation. This reduces the charge density on the material surface and, consequently, decreases the device's output performance.^[95,96] Additionally, the electric field established between the metal electrode and dielectric material can influence the output performance of the device by exerting a force on the inserted charges. Yi et al. found that the CS-TENG has a relatively lower built-in electric field than the SE-TENG. This contributes to higher V_{oc} , I_{sc} , and transfer charge, reducing the probability of air breakdown. As a result, the output performance of CS-TENG often surpasses that of SE-TENG. Furthermore, factors like the area of the triboelectric layer, the distance between the contact region and the external electric field, and changes in their relative orientations can all affect the electric field and, consequently, alter the output.^[65] Apart from the polarization effect, research indicates that the magnetization effect plays a significant role in the output of TENG. The periodic contact-separation motion of TENG generates alternating current, creating a magnetic field around the device that magnetizes a magnetic medium. Thus, theoretically,

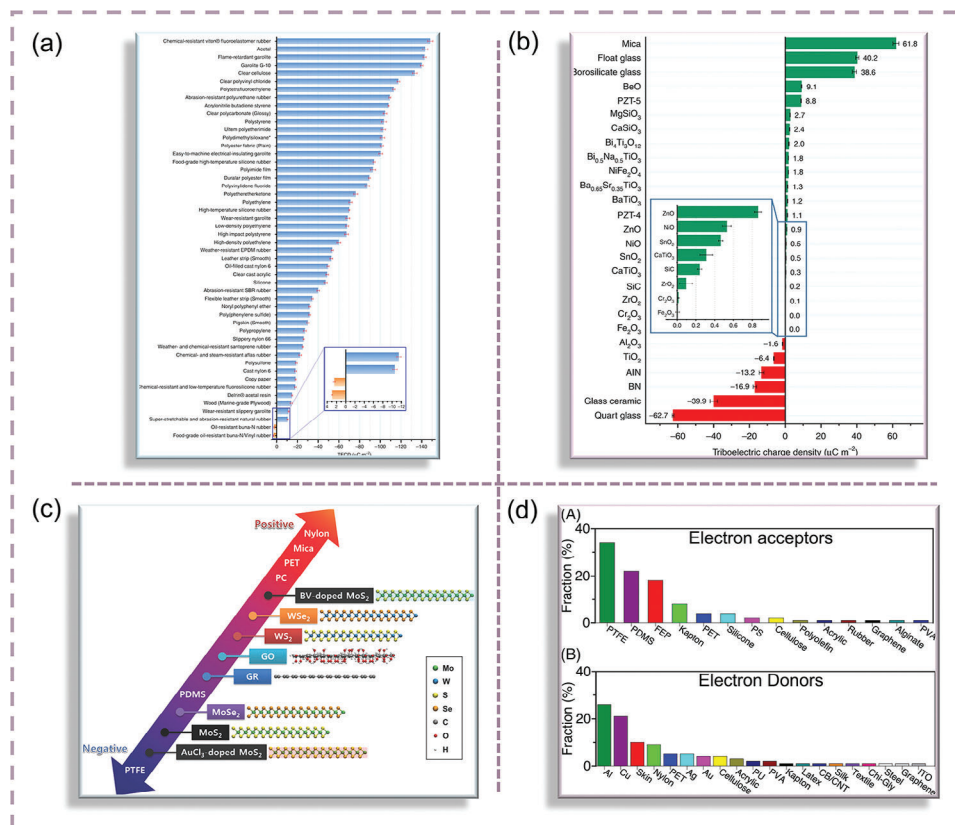


Figure 3. The triboelectric series and the statistics of triboelectric materials choices. a) The quantified triboelectric series mainly of polymers. Reproduced under terms of the CC-BY license.^[100] Copyright 2019, the Authors, published by Springer Nature. b) The quantified triboelectric series of some common inorganic nonmetallic materials. Reproduced under terms of the CC-BY license.^[99] Copyright 2020, the Authors, published by Springer Nature. c) The modified triboelectric series of 2D materials. Reproduced with permission.^[98] Copyright 2018, John Wiley and Sons/Wiley-VCH. d) The fraction (%) of the electron acceptor and donor materials used in 100 randomly selected articles from 2012 to 2020. Reproduced with permission.^[52] Copyright 2020, John Wiley and Sons/Wiley-VCH.

introducing a magnetic medium into TENG can generate a magnetization current and an electric field, enhancing the electrical output and energy conversion efficiency of TENG. In practice, TENGs based on ferromagnetic media are closely linked to the external magnetic field environment and exhibit higher output than TENGs based on non-ferromagnetic media.^[67]

3. Methods to Improve the Output Performance of TENG

This section presents the commonly used methods to enhance the output performance from five aspects: selection of triboelectric materials, materials surface modification, composite of material components, device structure design, and electrode modification.

3.1. Selection of Triboelectric Materials

The selection of triboelectric materials, widely spaced apart in the triboelectric series, can significantly enhance the output of TENG. The triboelectric series is determined based on the triboelectric polarity and TECD of different materials during CE.^[97–99]

The concept of the triboelectric series has been established for over 260 years. Since then, the library of triboelectric materials has continuously expanded, and related researchers have consistently explored related mechanisms over time. Polymers are commonly used in triboelectric layers due to their excellent dielectric properties.^[52] Specific materials such as polyamide and cellulose are often employed as tribo-positive materials because they strongly tend to lose electrons. On the other hand, materials like polytetrafluoroethylene (PTFE), poly(vinyl chloride) (PVC), and polydimethylsiloxane (PDMS), with high electronegativity, are frequently prepared as tribo-negative materials due to their ability to gain electrons. In 2019, Zou et al. introduced a universal standard method for quantifying the triboelectric polarization of various polymers. This method allowed for the uniform quantification of the surface triboelectrification of various materials using liquid metal. The normalized TECD revealed the intrinsic characteristics of materials for gaining or losing electrons. This method demonstrated a comprehensive ranking and quantification of the triboelectrification of materials (Figure 3a).^[100] Furthermore, in 2020, Zou et al. established a dedicated triboelectric series for inorganic nonmetallic materials and demonstrated that CE is an electronic quantum transition effect under ambient conditions. This study reveals that Mica is the most electropositive material,

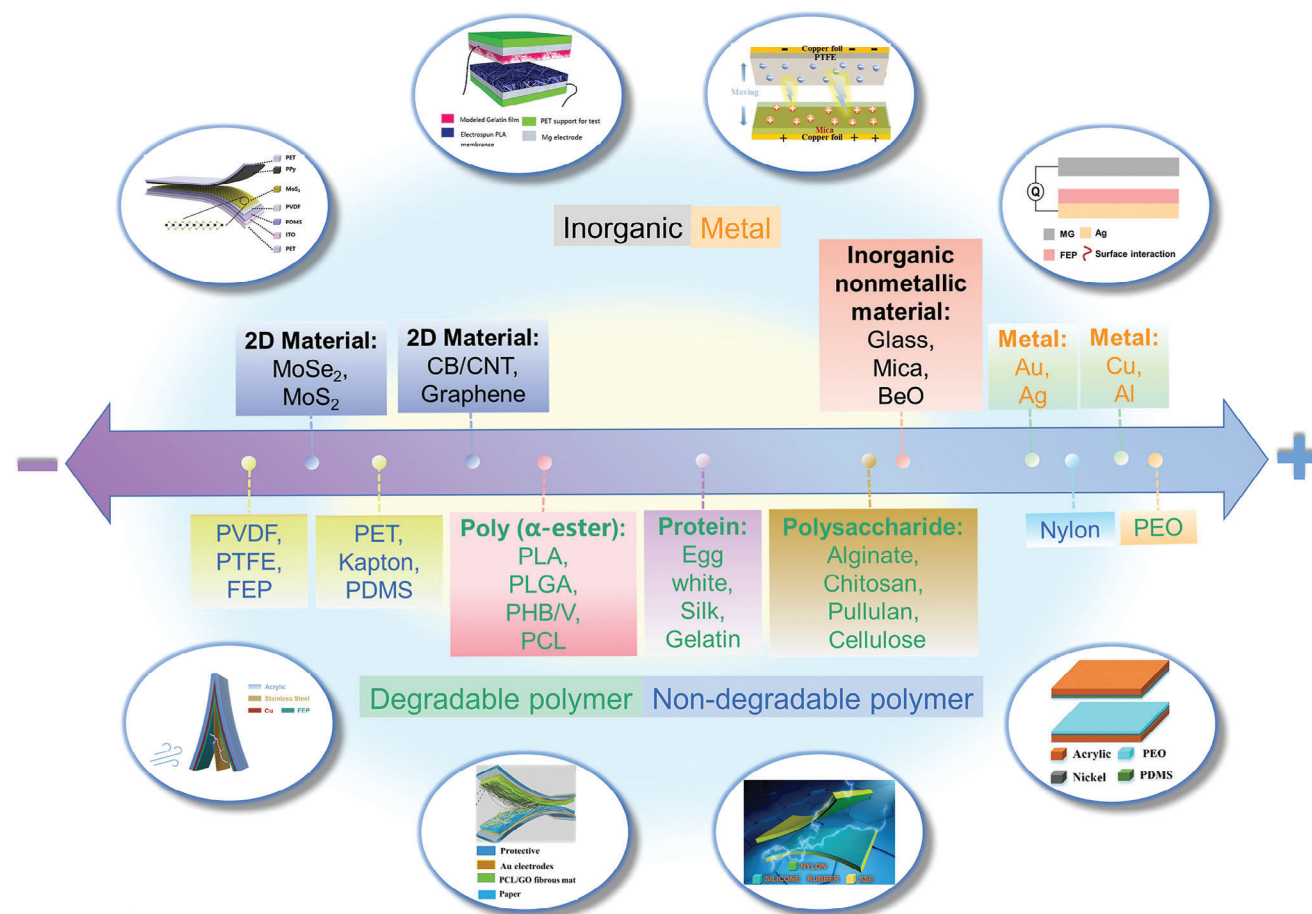


Figure 4. The triboelectric series of various typical materials and categories. 2D material MoS₂. Reproduced with permission.^[101] Copyright 2019, Elsevier. Gelatin and PLA. Reproduced with permission.^[102] Copyright 2018, Elsevier. Inorganic nonmetallic material Mica. Reproduced with permission.^[103] Copyright 2021, Elsevier. Metallic glass. Reproduced under terms of the CC-BY license.^[104] Copyright 2023, the Authors, published by Springer Nature. Cu and FEP. Reproduced with permission.^[105] Copyright 2022, John Wiley and Sons/Wiley-VCH. Poly(α -ester) material PCL. Reproduced with permission.^[106] Copyright 2019, Elsevier. Nylon. Reproduced with permission.^[107] Copyright 2020, John Wiley and Sons/Wiley-VCH. PEO. Reproduced with permission.^[108] Copyright 2018, Elsevier.

closely resembling the typical tribo-positive material nylon, while quartz glass is the most electronegative (Figures 3b and 4).^[99] In addition, Seol et al. also established a triboelectric series for 2D materials, including MoS₂, MoSe₂, WS₂, WSe₂, graphene, and graphene oxide (GO). These 2D materials, due to their strong EW ability, are mainly positioned near the tribo-negative PTFE and PDMS in the triboelectric series (Figures 3c and 4).^[98] Moreover, Zhang et al. conducted a comprehensive summary of triboelectric materials from 100 randomly selected articles, listing common electron donors (tribo-positive materials) and electron acceptors (tribo-negative materials). Notably, metals such as aluminum (Al), copper (Cu), silver (Ag), and gold (Au) exhibit electronegativity similar to nylon and are frequently used as tribo-positive materials (Figures 3d and 4).^[52] Based on a review of the literature survey and experimental results, we have compiled a rough triboelectric series for various typical materials and categories (Figure 4).

Polymers have become widely recognized as some of the most favored triboelectric materials due to their numerous advantages. These advantages include a wide range of categories, a significant

polarity difference in the triboelectric effect, and excellent stability. This section will discuss the detailed application of polymers as triboelectric materials. Among these, polyamides, such as nylon 6, stand out as one of the most extensively reported and positively charged triboelectric polymer materials.^[109–111] However, Ding et al. have found that degradable polyethylene oxide (PEO) tends to lose electrons more readily than polyamide-6 (PA6), resulting in a higher level of positive polarity. In the specific case of a PEO/PDMS TENG (2 × 2 cm²), which consists of a spin-coated flat PEO and PDMS film, they achieved notable results with a peak-to-peak V_{oc} of 970 V, a J_{sc} of 85 mA m⁻², and a peak power density of \approx 40 W m⁻². In comparison, the PA6/PDMS TENG only produced an output of 630 V, 30 mA m⁻², and \approx 18 W m⁻². This enhanced triboelectric behavior of PEO can be attributed to the abundant positively charged oxygen functional groups (-O⁻) on the main chain and the lower work function of PEO compared to PA6 (Figure 5a).^[108] Moreover, cellulose, the most abundant natural polymer on earth, is commonly used as a tribo-positive material due to its strong ED ability. Yao et al. were the first to apply cellulose to TENG in 2016. They utilized flexible and

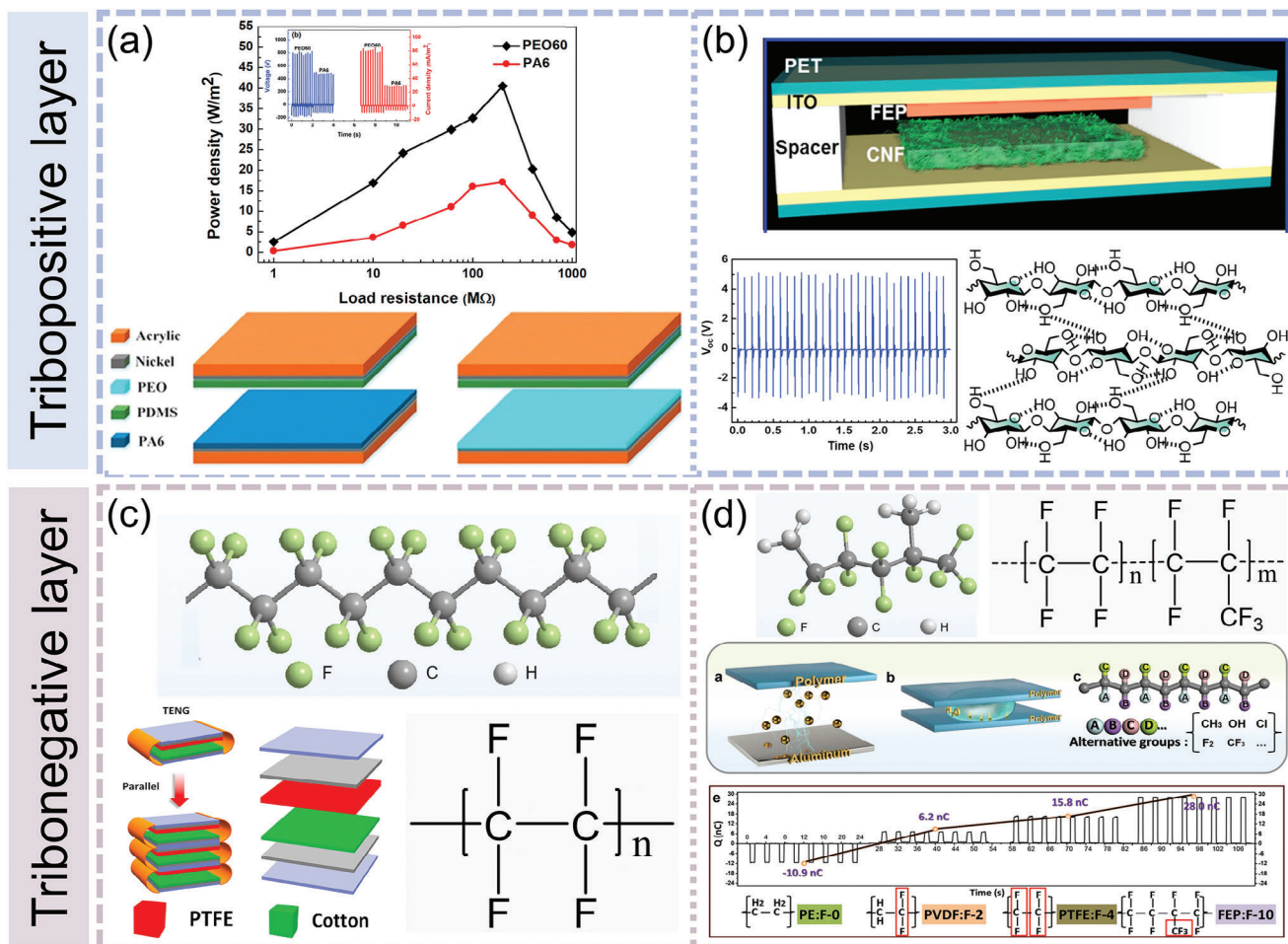


Figure 5. Several typical tribo-positive and tribo-negative materials. The tribo-positive materials include a) PEO. Reproduced with permission.^[108] Copyright 2018, Elsevier. b) Cellulose. Reproduced with permission.^[113] Copyright 2016, Elsevier. Reproduced under terms of the CC-BY license.^[120] Copyright 2023, the Authors, published by John Wiley and Sons/Wiley-VCH. The tribo-negative materials include c) PTFE. Reproduced with permission.^[114] Copyright 2021, Elsevier. d) FEP. Reproduced with permission.^[118] Copyright 2020, John Wiley and Sons/Wiley-VCH.

transparent cellulose nanofibrils (CNF) thin films as the tribo-positive layers. When paired with fluorinated ethylene propylene (FEP) to create a TENG device ($1 \times 1 \text{ cm}^2$), the average V_{oc} and I_{sc} peak values reached $\approx 5 \text{ V}$ and $\approx 7 \text{ } \mu\text{A}$, respectively. These values are comparable to the performance of TENGs that utilize typical synthetic polymer pairs such as Kapton (PI)-PET^[11] and PTFE-polyamide.^[112] The excellent output results from cellulose are due to its richness in oxygen atoms, known for their strong ED properties, thus making CNF films positively charged (see Figure 5b).^[113] Additionally, biodegradable polymers, including polysaccharides, proteins, and polyesters, contain abundant functional groups like hydroxyl, amino, and ester groups, which enhance their ability to lose electrons, resulting in the favorable property being positively charged. The positions of these materials sit close to nylon in the triboelectric series (Figure 4). Importantly, these biodegradable polymers have gained significant attention due to their outstanding biosafety and environmental friendliness. Regarding tribo-negative layers, PTFE is frequently used because of its abundance of electronegative fluorine (F) atoms (Figure 5c).^[114–117] However, Li et al. found that FEP, which

contains a higher density of F atoms, exhibits a greater EW ability than PTFE. They have also noted that triboelectric negative polarities increase with increasing the density of F or chlorine atoms in the molecule and obey the following order (from weak to strong in negative polarity): polyethylene < PVC < poly(vinylidene difluoride) (PVDF) < PTFE < FEP (Figure 5d).^[118] The ED or EW ability of main- and side-chain chemical groups of the polymer and their density determine the triboelectric polarity of the molecule.^[119] Polymers with chemical groups like polyether group, carboxylate group, amine group, hydroxyl group, amide group, and ester group tend to possess positive polarity, while those with unsaturated bonds, fluorine, and chlorine atoms usually show negative polarity.

3.2. Materials Surface Modification

The methods for material surface modification are primarily categorized into three groups based on different mechanisms. These categories include surface chemical bond variation, the

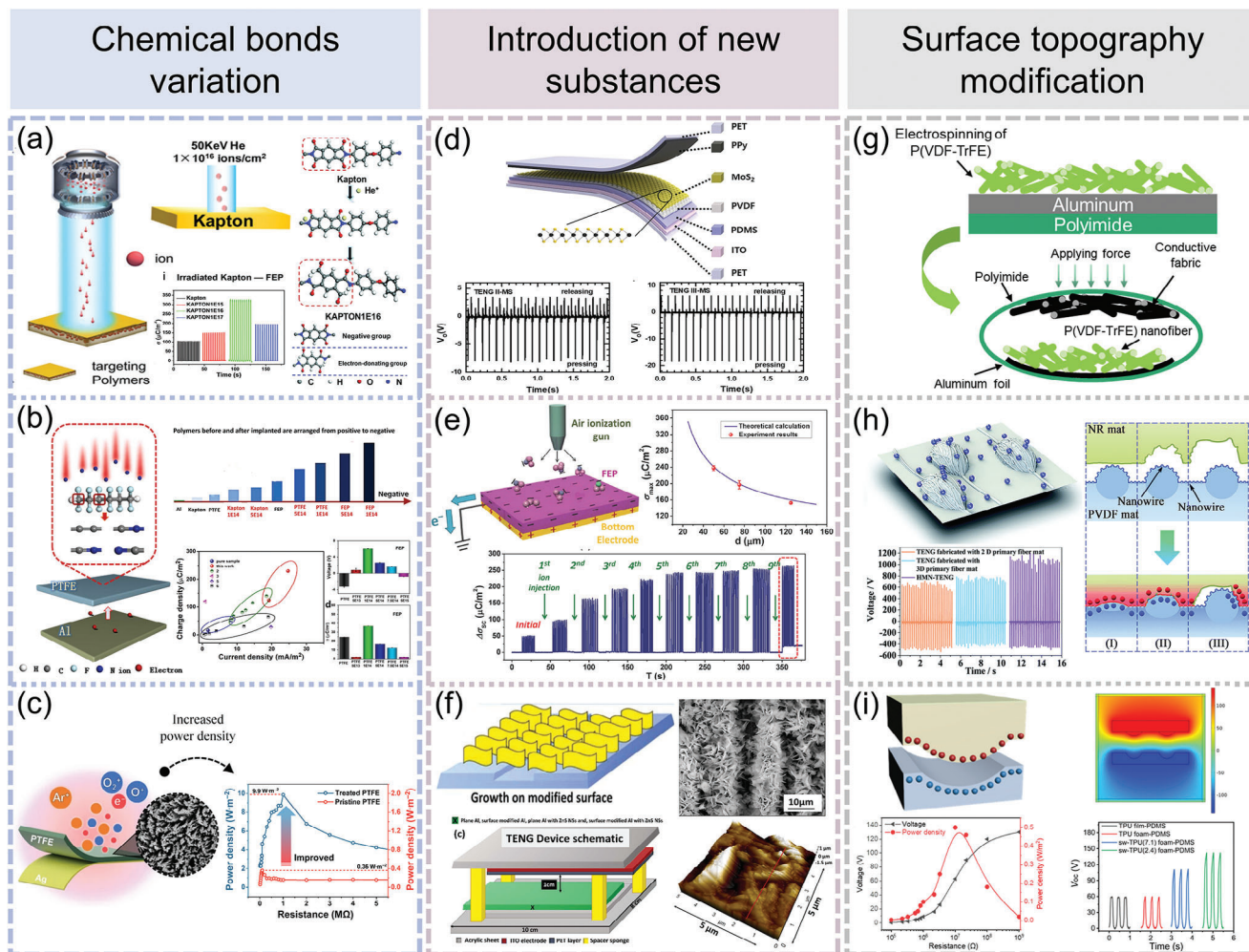


Figure 6. Triboelectric materials surface modification methods are divided into three types, which are related to chemical bond variation through a) low-energy helium (He) ion irradiation. Reproduced with permission.^[122] Copyright 2020, Royal Society of Chemistry. b) Nitrogen (N) ion implantation technology. Reproduced with permission.^[123] Copyright 2021, Elsevier. c) A two-step or sequential O₂/Ar plasma treatment via inductively coupled plasma etching. Reproduced with permission.^[124] Copyright 2022, Springer Nature. The introduction of new substances includes d) a large-sized MoS₂ monolayer. Reproduced with permission.^[101] Copyright 2019, Elsevier. e) Single-polarity charged particles/ions. Reproduced with permission.^[51] Copyright 2014, John Wiley and Sons/Wiley-VCH. f) ZnS nanosheet arrays. Reproduced with permission.^[126] Copyright 2022, Elsevier. Surface topography design includes g) a honeycomb-like nanofiber network. h) A 3D secondary heart-like structure. Reproduced with permission.^[128] Copyright 2019, Royal Society of Chemistry. i) Surface wrinkly structures. Reproduced with permission.^[129] Copyright 2023, John Wiley and Sons/Wiley-VCH.

introduction of new substances, and surface topography alterations. Each of these modification methods aims to enhance either the ED or EW capability of the material while also increasing its specific surface area of the material, which is conducive to enhancing the amount of charge transfer between the triboelectric layers, thereby improving the output performance of TENG:

As the chemical potential of organic polymeric materials is directly related to their functional groups, surface potential can be effectively controlled by introducing suitable functional groups exposed on the surfaces without altering the bulk material and its fundamental properties.^[121] Li et al. devised a surface modification strategy using low-energy helium (He) ion irradiation to tune the chemical structures and functional groups of triboelectric polymers directly at the molecular level. The He ion was chosen as an implantation ion due to its high electronegativity and stability. This method effectively stabilizes the electrification

performance of the material surface to a depth of tens of nanometers while making minimal changes to surface roughness at the micro-scale and the mechanical flexibility of the target polymer. In a CS-TENG, with a contact area of 49 mm², constructed using the modified PI and a typical FEP film, the SCD reached up to 332 μC m⁻² and a maximum peak power of 18 μW under normal environmental conditions. This output is much higher than the reference TENG using the common PI film, which only achieves 0.5 nW. The He ion irradiation led to the breaking of C—N bonds and the formation of aldehyde (—CHO) and amide (—NHCOR) groups on the surface of the target PI film. The conjugation effect of the —NHCOR bond and the benzene ring generated a powerful group to produce more electrons (Figure 6a).^[122] A nitrogen (N) ion implantation technology was also employed to regulate the electrification properties of tribo-negative materials PTFE and FEP precisely. The implanted N ions disrupted chemical bonds

in PTFE and FEP films and generated stronger polar bonds between atoms, such as $C\equiv N$ or $C=N$. This broke the spatial structural symmetry of PTFE, turning it into a polar polymer while also increasing the density of the electron cloud of functional groups and enhancing its EW ability. The modified PTFE and FEP demonstrated 7.8- and 4.6-fold higher transfer charge densities than the original samples, reaching 125 and 230 $\mu C m^{-2}$, respectively (Figure 6b).^[123] Recognizing the toxicity of CF_4 to humans and the environment, Prada et al. introduced a surface modification method for PTFE, using a two-step or sequential O_2/Ar plasma treatment via inductively coupled plasma etching without using CF_4 gas. The plasma treatment did not change the internal structure of PTFE but instead modified only the surface structure. Chemical bond defects with surface trapping charges generate additional polarization due to defect dipole moments under an applied electric field, leading to an increased dielectric constant of the plasma-treated PTFE samples. The O_2/Ar plasma-treated PTFE-TENG achieves a superior power density of 9.9 $W m^{-2}$, almost 30 times higher than that of a pristine PTFE-TENG. The intensified TECD and the enhancement of power output of PTFE-based TENG can be attributed to the synergistic combination of high surface area and charge trapping sites resulting from a sequential O_2/Ar plasma (Figure 6c).^[124]

Introducing monolayers, ions, or structured new substances on the surface can also significantly affect the material's work function, surface potential, and roughness, thus directly altering the material's electronegativity. First, depositing a particular monolayer on the material's surface is a practical modification strategy. Kim et al. developed a method using chemical vapor deposition to grow a large-sized MoS_2 monolayer. Compared to ohmic contact, TENGs with the Schottky contact and pn junction generated higher output power. The TENGs without MoS_2 , with top layers of indium tin oxide (ITO)/PET (ohmic contact), Au/PET (Schottky contact), and polypyrrole (PPy)/PET (pn junction), exhibited almost symmetric alternating current outputs with a $|V_o|$ of 2.5–5 V. Nevertheless, after adding MoS_2 in the bottom layer, the TENGs with top Au/PET and PPy/PET layers presented higher V_{oc} and asymmetric outputs, reaching a maximum of ≈ 8 and ≈ 18 V, respectively. This is attributed to the diffusion of charges, which leads to the formation of a depletion layer across the Schottky or pn junction (Figure 6d).^[101] Also, Ma et al. reported a surface modification method based on poly(vinylidene fluoride-co-trifluoroethylene) (P(VDF-TrFE)) deposited Langmuir monolayer, which improved the output performance of TENG more than 15 times. The dipolar moments of C–F and C–H bonds in P(VDF-TrFE) fluoropolymer collectively generate compelling dipolar moments perpendicular to the carbon main chain and along the direction of the chain, which causes a significant downward shift of the Fermi level. Hence, the ITO surface modified by P(VDF-TrFE) Langmuir monolayer polymer exhibits a more negative contact potential and a larger work function, indicating a more significant EW ability.^[125] Moreover, ion implantation is a straightforward and efficient modification method that can rapidly increase the SCD of materials, thus providing a powerful driving force for high output power. In 2014, Wang et al. proposed a novel process for generating surface charges by using an air-ionization gun to inject single-polarity charged particles/ions onto the surface of an electret. Through adjusting the injection cycles, the SCD can be directly controlled

to reach any desired level possibly. Through repeatedly injecting negative ions onto the surface of FEP multiple times, the negative charges gradually accumulate, and the final SCD can reach $\approx 630 \mu C m^{-2}$, which is over ten times higher than the SCD achievable with electrode-free dielectric films (53.1 $\mu C m^{-2}$). Simultaneously, the output power is elevated by as much as 25 times (Figure 6e).^[51] ZnS is a material that possesses piezoelectric and triboelectric properties and holds the advantages of availability of precursors, ease of preparation, and chemical stability. Moreover, it enables nanostructure growth at low temperatures. Through hydrothermal growth, ZnS nanosheet arrays were fabricated and introduced on the surface-modified Al substrate, significantly improving the charge transfer rate and the effective contact area between triboelectric pairs. The modified TENG with ZnS exhibits an output power density of $\approx 1.325 W m^{-2}$, a V_{oc} of ≈ 262 V, and an I_{sc} of $\approx 56 \mu A$, respectively, which are ≈ 4.6 and 5 times higher than the plane Al-based TENG (Figure 6f).^[126]

Surface micromorphology exerts a great impact on the triboelectric effect. The introduction of microstructures can increase the effective contact area, thus improving the output performance. Electrospinning is a simple method to create rough material surfaces. Jang et al. found that using a specific concentration of P(VDF-TrFE) solution, a honeycomb-like nanofiber network could be generated solely through electrospinning without additional processing. Compared with a typical flat nanofiber network-based TENG, the power density of honeycomb-like nanofiber-based TENG was enhanced more than twofold by 1.6 $W m^{-2}$ due to the large surface area and high surface roughness of the honeycomb structure (see Figure 6g).^[127] Moreover, Zhang et al. demonstrated a heart-like micro-nanofiber-based TENG with high performance. A 3D secondary heart-like structure was self-assembled on an electrospun PVDF fiber-based tribo-negative layer, which could match the depressed porous and ravine-like structures on the tribo-positive layer. The joint effect between the heart-like and the porous structure enlarges the effective contact area because of their high surface roughness and the "occlusion effect." The fabricated TENG can deliver the current density of 97 $mA m^{-2}$ and the power density of 14.8 $W m^{-2}$, which are 1.6 and 1.4 times those of TENGs comprising the typical 2D primary nanofiber mat and the 3D primary micro-nanofiber mat, respectively (see Figure 6h).^[128] Additionally, a dynamic supercritical carbon dioxide ($scCO_2$) foaming method was proposed to introduce a $scCO_2$ flow field during $scCO_2$ saturation to fabricate thermoplastic polyurethane (TPU) foams with surface wrinkly structures. The generation of surface wrinkles is attributed to the combination effect of volumetric expansion and intramolecular stress relaxation induced by the CO_2 expansion and the $scCO_2$ flow field. The size of the surface wrinkles can be regulated within the range of 1.8–10 μm by adjusting the foaming pressure. The TPU film with a wrinkle wavelength of 2.4 μm , combined with a structured PDMS film, demonstrates the maximum V_{oc} , transfer charge, and I_{sc} of 141 V, 46 nC, and 2.8 μA , respectively, which are 130%, 180%, and 130% higher than the conventional TENG (Figure 6i).^[129] In addition, Li et al. utilized a template-based etching method to fabricate a porous PDMS triboelectric layer with an anti-nickel foam structure, which served as the tribo-negative material for a fully stretchable TENG. This microstructure improves the surface-to-volume ratio and surface

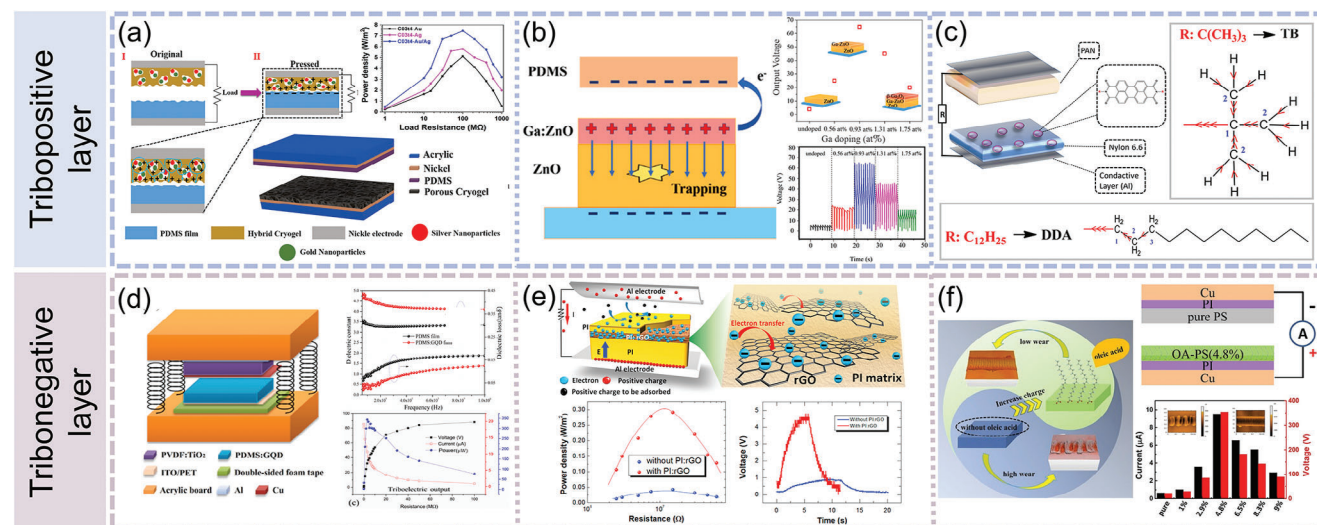


Figure 7. Doping other substances into triboelectric materials. Tribo-positive layers include a) the porous hybrid bimetallic cryogel film containing Ag and Au nanoparticles. Reproduced with permission.^[131] Copyright 2020, John Wiley and Sons/Wiley-VCH. b) The Ga-doped ZnO thin film. Reproduced with permission.^[132] Copyright 2021, Elsevier. c) The nylon 6,6 (PA66) films containing two PDI-based organic materials. Reproduced with permission.^[135] Copyright 2022, John Wiley and Sons/Wiley-VCH. Tribo-negative layers include d) the PDMS triboelectric layer modified by graphene quantum dots (GQDs). Reproduced with permission.^[136] Copyright 2021, Elsevier. e) The PI triboelectric layer embedded with reduced graphene oxide (rGO) as electron-trapping sites. Reproduced with permission.^[137] Copyright 2017, Elsevier. f) Polystyrene (PS) triboelectric pair with the addition of oil-acid (OA). Reproduced with permission.^[139] Copyright 2020, Elsevier.

roughness, resulting in the output voltage tenfold higher than the TENG based on a flat PDMS film.^[130]

3.3. Composite of Material Components

In the quest to optimize the output of TENG devices, a critical focus is placed on altering the composition and proportions of the triboelectric layer components through doping metal particles, inorganic substances, organic molecules, and other additives into the triboelectric materials. These additions modify the ED capability and the microstructure of the overall bulk material, thereby inducing changes in key parameters like relative permittivity (ϵ_r), electrical conductivity, and TECD. As a result of these modifications, the charge transfer capability of these enhanced triboelectric materials significantly improves under the same friction conditions. This, in turn, leads to a substantial enhancement in the output performance of TENG devices.

Incorporating fillers like metal particles and organic molecules into tribo-positive materials is straightforward to heighten their triboelectric performance. Haleem et al. fabricated a porous hybrid bimetallic cryogel film containing Ag and Au nanoparticles as the tribo-positive material of a TENG device. Through pairing with PDMS as the opposite (with a dimension of $1 \times 2 \text{ cm}^2$), it produced an output voltage of 262.14 V, much higher than the pure cryogel film-based TENG of 162.26 V. The porous and rough structure interaction of nanoparticles introduced in the hybrid cryogel contributes to the performance enhancement of the tribo-positive material, which allows it to compress upon applying external force in contact with the tribo-negative layer. Therefore, the total contact area between the two layers increases. The metal nanoparticles can donate electrons through the contact surface to improve the SCD, and their rough structure increases the

depth of the triboelectric layer (as shown in **Figure 7a**).^[131] Additionally, the Ga-doped ZnO thin film as the tribo-positive layer benefits the output performance of TENG significantly. The output voltage and current of the ZnO film doped with 0.93 at.% Ga can be drastically enhanced by 16 and 13 times, respectively. The enhanced performance of TENGs stems from the synergistic effects of increased free carriers at the surface due to the Ga doping and enlargement of work function difference by upward shifting of the Fermi level of ZnO. Except for the increased work function difference, through Ga doping into ZnO, the limited depth of Ga diffusion helps to preserve the rest of the bulk ZnO remaining insulating, which serves as a charge trapping layer to suppress recombination of triboelectric charges with induction charges, further facilitating the performance of TENG. This study provides valuable insights for optimizing the electronic structure of semiconductors (see **Figure 7b**).^[132] Alongside inorganic doping,^[133,134] Yiğit Arkan et al. doped two different perylene diimide (PDI)-based organic structures into triboelectric layers and demonstrated that these two PDI-based organic materials could increase the tribo-positive charge density and the output power of TENG. Two different side chains were introduced to modify the main PDI backbone. The results demonstrated that doping 1 wt.% of 2,9-di-tert-butylanthra [2,1,9-def:6,5,10-d'e'f'] diisoquinoline-1,3,8,10(2H,9H)-tetraone (TB) and 2.5 wt.% of 2,9-didodecylanthra [2,1,9-def:6,5,10-d'e'f'] diisoquinoline-1,3,8,10 (2H,9H)-tetraone (DDA) into nylon 6,6 (PA66) can elevate the device performance by 3.3 times and achieve the optimal result of 500 V. TB exhibits higher electron donor characteristic than DDA due to the presence of methyl pairs on the main backbone, which enhances the electron density of molecules and reduces the oxidation potential. The achievement obtained in this study suggests that even minor alterations in side chains of molecular structure can lead to remarkable changes in a

substance's electrochemical properties, improve the nanofibers' structural properties, and result in the variation of fabricated device parameters. The results confirm that organic doping reaching a certain level can increase the TECD of the dielectric material, thus enhancing the output efficiency (Figure 7c).^[135]

Similarly, doping also applies to tribo-negative materials, such as inorganic nanoparticles, 2D materials, and organic compounds. Specifically, Yang et al. prepared a polymer-based hybrid piezoelectric-triboelectric nanogenerator, in which the PDMS triboelectric layer was further modified by graphene quantum dots (GQDs). The doped conductive GQD in the PDMS matrix presents excellent dispersion and does not significantly affect its transparency. On the one hand, the GQD particles significantly increase the permittivity of PDMS film while the dielectric loss is reduced to a certain degree. Consequently, more polarized tribocharges are generated on the surface during contact friction. On the other hand, the GQD particles form numerous microcapacitors within the PDMS substrate, thus reducing the effective thickness of the PDMS dielectric film. As a result, the V_{oc} of the triboelectric part enhances to 105 V with an increase of 102%, indicating that GQD modification in PDMS effectively improves the triboelectric output (see Figure 7d).^[136] 2D materials possessing unique structures and properties have been widely used in the research of TENGs. To facilitate the charge transfer, Wu et al. incorporated reduced graphene oxide (rGO) as electron-trapping sites into PI as the tribo-negative layer, in which rGO sheets embedded in the PI layer could efficiently capture the friction-generated electrons. This hybrid layer suppressed the recombination between electrons and tribo-positive charges, achieving a higher density of triboelectric electrons and voltage output. The maximum power density of the CS-TENG with the PI:rGO layer reaches 6.3 W m^{-2} , which is 30 times as large as that of the TENG without the PI:rGO layer (Figure 7e).^[137] In addition, Wang et al. incorporated 2D MXene ($\text{Ti}_3\text{C}_2\text{T}_x$) into the PDMS tribo-negative layer. The outstanding electrical conductivity of metallic MXenes notably reduces the composite film's resistance. Moreover, its unique 2D structure increases the specific surface area of the PDMS film. The abundant -F groups on the MXenes surface also possess strong electron adsorption ability. These properties all make MXene-doped TENG achieve an impressive output power of 104.87 W m^{-2} , far surpassing the graphene-doped TENG (10.10 W m^{-2}) as well as the pure PDMS-based TENG (4.85 W m^{-2}) prepared under the same conditions.^[138] Furthermore, small organic molecules have aroused great interest due to the simpleness of production, undemanding purification process, well-defined molecular weight, tunable electronic structure, and excellent reproducibility. Zhang et al. designed an oil-acid (OA)-enhanced TENG with high output performance and wear resistance. On the one hand, OA enhances the electronegativity of the polystyrene (PS) triboelectric layer. On the other hand, OA acts as a lubrication additive to reduce the friction coefficient and wear volume by $\approx 90\%$ compared to pure PS. According to Pauling electronegativities, the group electronegativity value of $-\text{COOH}$ is higher than that of $-\text{C}_6\text{H}_5$, implying OA has a stronger ability to attract shared electron pairs than PS. The doped OA can modify the triboelectric polarity and charge retention ability of the PS thin film, thereby enhancing the total charge capacitance of PS-OA film and significantly improving the output performance of TENGs. The maximum output

power of the PS-based TENG reaches $470.5 \mu\text{W}$ with OA addition of 4.8 wt.%, which is 79 times larger than the device without OA doping (Figure 7f).^[139] Besides, the method of composite incorporation of organic high-molecular-weight polymers can also come into effect. Liu et al. successfully fabricated a susceptible and self-powered acid rain sensor based on a TENG by incorporating PDMS into PTFE. The PTFE-PDMS composite film from the spin-coating process exhibits enhanced surface hydrophobicity, with a larger quantity of electrons transferred, larger surface roughness, and significantly improved permittivity. Compared with the output differences ($6.67 \mu\text{A}$ and 14.3 V) of a pristine device with PTFE film, the sensor with the PTFE-PDMS film is enhanced to $26.37 \mu\text{A}$ and 69.04 V .^[140]

3.4. Structural Design

Numerous derived, composite, and innovative structures have arisen based on the five fundamental operating modes of TENG. These devices not only outperform individual devices in terms of output current, voltage, and power density but also effectively harness diverse forms of mechanical energy from the environment. This wide adaptability caters to a broad spectrum of application scenarios. To evaluate the performance of TENGs, Zi et al. introduced a universal standard known as the figure-of-merits for performance evaluation of TENGs (FOM_p). FOM_p comprises a structural figure-of-merit (FOM_s) related to the device's structure and a material figure of merit (FOM_M), which is the square of the SCD.^[97] These figure-of-merits confirm how the device's structure impacts its output. This section elaborates on the advancements in TENG structural modification from two perspectives: the addition of functional layers and the transformation of the entire configuration, respectively.

Adding functional layers to the basic device structure can significantly improve the output performance. The core components of a TENG consist of the triboelectric layer and the electrode layer. Embedding an intermediate layer between the triboelectric layer and the electrode, or between two triboelectric layers, is one of the effective strategies to optimize the charge storage of triboelectric materials, suppress charge decay, and enhance the induced potential. In 2016, Cui et al. introduced the concept of incorporating a functional intermediate layer into the triboelectric layer as a novel strategy. This can be achieved through methods such as sputtering metal, coating with an organic polymer layer, or adding a charge supplement to extend charge decay time, enhance induced charge, and improve the output performance of TENG.^[58] Metals are especially suitable for this purpose due to their high electron density and electrical conductivity, making them ideal for use as both electrode materials and intermediate layers. For instance, Lai et al. employed Au as an intermediate layer, embedding it between a PDMS layer and the bottom Al electrode, resulting in an Au-PDMS TENG. By introducing ravines and gullies in criss-crossed Au layers, electron trapping tunnels were created, increasing the likelihood of electron tunneling from PDMS to the Au layer. The results show that the formation of an internal-space-charge zone at the Au-PDMS interface, facilitated by the ravines and gullies, directly enhances the electrical output of the TENG, leading to a transfer charge density of $168 \mu\text{C m}^{-2}$, nearly four times the value of a pure

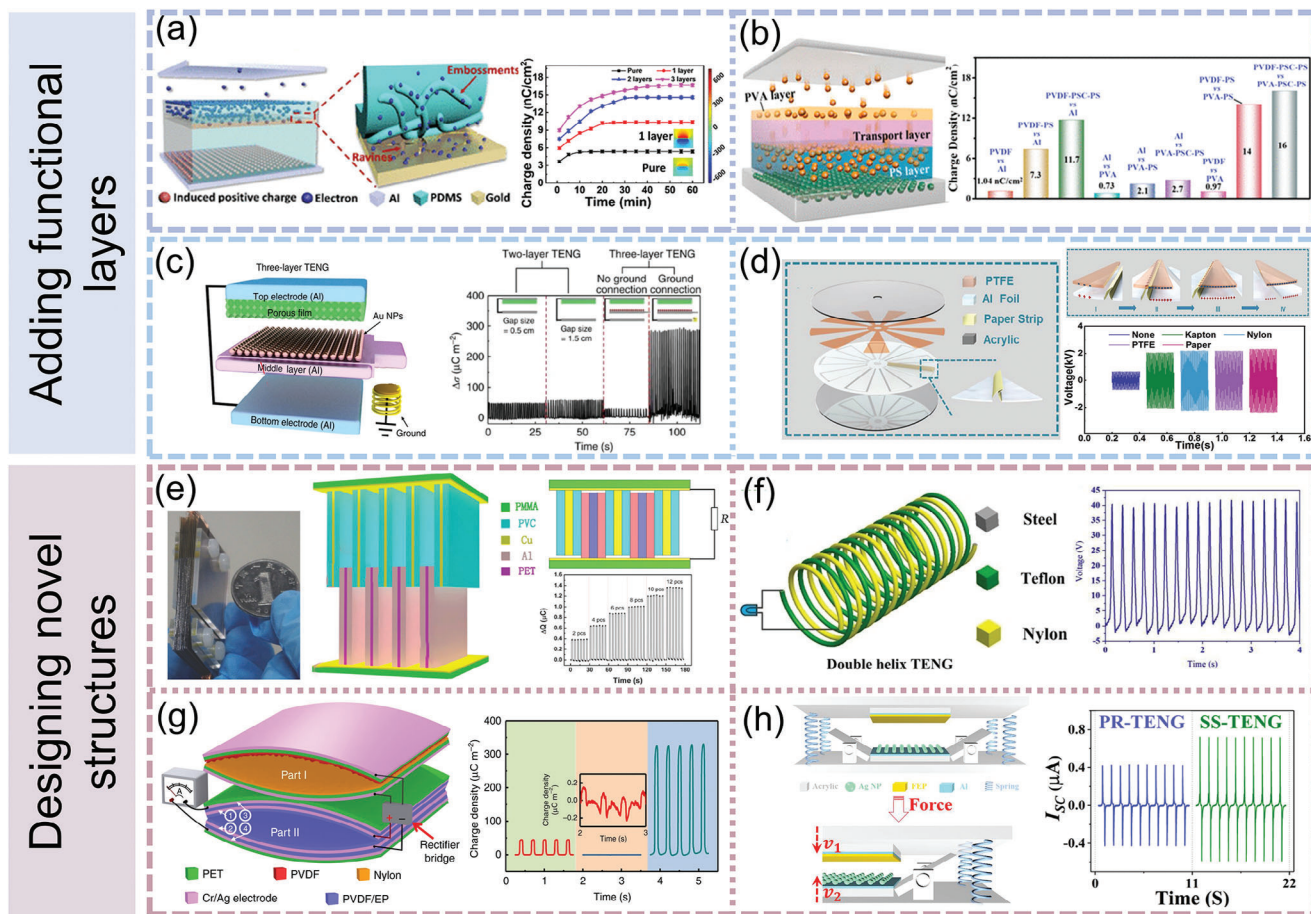


Figure 8. Structural optimization of TENG devices. Adding functional layers includes a) embedding the Au intermediate layer between the PDMS and the bottom Al electrode. Reproduced under terms of the CC-BY license.^[141] Copyright 2018, the Authors, published by American Chemical Society. b) A three-layered composite structure (TLCS) as the tribo-positive layer. Reproduced under terms of the CC-BY license.^[142] Copyright 2018, the Authors, published by American Chemical Society. c) Inserting a middle layer with Al film coated by Au nanoparticles between a top and a bottom layer. Reproduced under terms of the CC-BY license.^[145] Copyright 2016, the Authors, published by Springer Nature. d) Adding a small paper strip as an intermediate layer. Reproduced with permission.^[146] Copyright 2021, John Wiley and Sons/Wiley-VCH. Designing composite or novel structures includes e) a 3D multi-layered sliding TENG (3D-TENG) of layer-by-layer stacked structure. Reproduced with permission.^[147] Copyright 2014, John Wiley and Sons/Wiley-VCH. f) A double-helix TENG (DH-TENG). Reproduced with permission.^[148] Copyright 2021, Elsevier. g) A self-improving TENG (SI-TENG) with an inner plane-parallel capacitor structure (PPCS). Reproduced under terms of the CC-BY license.^[50] Copyright 2018, the Authors, published by Springer Nature. h) A seesaw-structured TENG. Reproduced with permission.^[149] Copyright 2019, Elsevier.

PDMS-based TENG (as shown in **Figure 8a**).^[141] Furthermore, a three-layered composite structure (TLCS) was designed for the tribo-positive layer. This TLCS consists of three sublayers stacked from the outermost to the bottom: a charge collection sublayer (CCL) on the surface, a charge transport sublayer (CTL) containing a small number of carbon nanotubes, and a charge storage and barrier sublayer (CSBL). Each sublayer has a distinct role in enhancing the performance of TENG. The CCL is responsible for efficiently capturing tribo-positive charges from the tribo-negative layer. The CTL is designed to transport the generated triboelectric charge deeper into the structure. The CSBL plays a crucial role in holding and storing more charges. The combined effect of these sublayers creates a transport channel that effectively increases the distance between the triboelectric charges and the triboelectric layer's surface. This adjustment helps weaken the repulsion between the first entered charges and the later entered positive charges. Using a multi-layer composite structure

increases the charge density by 3.7 times for the tribo-positive layer of TENG. When this multi-layer composite structure is applied to the tribo-positive and tribo-negative layers simultaneously, the charge density can be raised by 16.5 times (as illustrated in **Figure 8b**).^[142] Moreover, incorporating a buffer layer at the bottom of the triboelectric layer provides favorable conditions for charge transfer. In a novel TENG that utilized a Pt-free carbon material, a sponge layer served as a buffer layer, ensuring intimate contact between the triboelectric layers. Introducing this buffer layer to the precharged TENG enhances output power stability. This multi-layer linkage TENG achieves an increased output current from 0.25 to 1.2 mA, a voltage from 700 to 1300 V, and a stable peak power density of 7.4 W m⁻².^[143] Han et al. employed hexagonal boron nitride (h-BN) nanosheets as a buffer layer and deposited a high-k dielectric material, Al₂O₃, with a high charge storage capacity on graphene. This polymer buffer layer mitigates the potential damage to the graphene lattice

and prevents possible oxidation during the atomic layer deposition of Al_2O_3 . Applying the $\text{Al}_2\text{O}_3/\text{h-BN}/\text{graphene}$ multi-layer structure to TENG results in an output voltage of 1.2 V and an output current density of 150 nA cm^{-2} under a vertical compressive force of 1 kgf. In contrast, the $\text{Al}_2\text{O}_3/\text{graphene}$ -based TENG without h-BN hardly generates any output.^[144] Additionally, incorporating dual-layer structures and charge supplements between the triboelectric layers represents another innovative approach. A practical three-layer TENG was reported, inserting a middle layer with an Al film coated by Au nanoparticles between a top layer with a mesoporous dielectric film on the top Al electrode and a bottom Al layer. This TENG ingeniously combines the CS mode and SE mode. The sequential contact configuration of TENG and direct electrical connection of the middle layer to the earth effectively induces efficient charge separation in the middle layer. When an external force is applied to the top layer, the charge density of both the top and bottom layers increases. As the force is withdrawn, three layers are simultaneously separated, and the enhanced potential allows more electrons to flow through the circuit. This results in a sustainable and enhanced output performance, generating 1.22 mA and 46.8 mW cm^{-2} , a more than 16-fold improvement over traditional TENGs (as depicted in Figure 8c).^[145] Notably, using an intermediate layer between triboelectric layer pairs is not limited to metallic materials. Bai et al. developed a freestanding rotary TENG (rTENG) with an intermediate layer. By simply adding a small paper strip to the conventional structure, the voltage output triples to 2.3 kV, while the current and charge output quintuple to 133 μA and 197 nC, respectively. The easily accessible and cost-effective paper strip functions as a super-effective charge supplement, generating a higher output voltage than other materials such as PI, nylon, and PTFE. Moreover, it exhibits exceptional durability. This enhancement strategy's key mechanism lies in the paper's propensity to carry positive charges, enabling significant charge supplementation to the tribo-negative layer of PTFE and, consequently, increasing the device's output (as shown in Figure 8d).^[146]

In addition to incorporating functional layers, various composite and innovative structured devices have been developed, such as parallel placement, double-helix, inner plane-parallel capacitors, and seesaw structures, among others. These innovations enhance the output and cater to diverse application scenarios. First, connecting sets of single devices in parallel is a simple, feasible, and highly effective approach. Du et al. employed layer-by-layer stacked PVC and Al as triboelectric materials to demonstrate a 3D multi-layered sliding TENG (3D-TENG). The results reveal that the output of the 3D-TENG effectively improves with an increase in triboelectric layers. The transfer charge increases from 0.4 to $1.37 \mu\text{C}$ as triboelectric layers increase from 2 to 12. In the case of a 3D-TENG consisting of 20 layers of PVC and Al, respectively, the device can reach a V_{oc} of 800 V, a peak short-circuit current density (J_{sc}) of 5.5 mA m^{-2} , a peak power density of 4.4 W m^{-2} , and a maximum charge transfer quantity of $2.6 \mu\text{C}$. This 3D-TENG can be considered multiple individual planar TENGs connected in parallel. This configuration significantly increases the friction area within the same space, making generating charge in the circuit easier and enhancing the output current (see Figure 8e).^[147] Additionally, a recent introduction is the double-helix TENG (DH-TENG). The DH-TENG utilizes two identical and intertwined steel springs as the sup-

port structure and electrodes, coated with triboelectric materials of opposite polarities, such as nylon and Teflon. This structural design substantially reduces the cost of TENG and significantly improves the synchronization effect during contact separation. By doubling the contact area of the triboelectric layer, the DH-TENG maximizes space utilization and charge generation. The prototype DH-TENG provides a V_{oc} of 42.9 V, an I_{sc} of 1.8 μA , and a peak power density of $8.87 \mu\text{W cm}^{-3}$ (see Figure 8f).^[148] Unfortunately, the charge density of TENG is mainly restricted by air breakdown. To overcome this limitation, Cheng et al. devised a self-improving TENG (SI-TENG) with an inner plane-parallel capacitor structure (PPCS) aimed at enhancing the TENG's output performance. The SI-TENG comprises two parts: Part I, which operates in CS mode and generates high voltage under vibration and transfers charge into the PPCS, and Part II, which includes two PET films and corresponding covered electrodes to create the PPCS. The charges generated by Part I are stored in the PPCS, resulting in a high charge density. When driven by vibration, the SI-TENG produces electrical output, achieving a maximum effective charge density of $490 \mu\text{C m}^{-2}$. Compared to the output of Part I, the output current and voltage of SI-TENG increase from 5.6 μA and 460 V to 57.8 μA and 922 V, respectively. The effective charge density also improves from 45 to $325 \mu\text{C m}^{-2}$ (see Figure 8g).^[50] Furthermore, Lin et al. introduced a seesaw-structured TENG based on the CS mode. In this device, the top and bottom triboelectric units are connected to two seesaw-structured linkages through flexible connectors. When external force drives the top triboelectric unit downward, it triggers the seesaw-like linkages to lift the bottom triboelectric unit, causing both tribo-surfaces to participate in relative motion, thereby enhancing relative motion velocity. Compared to the previously reported CS-TENG, the I_{sc} and the power density increase from 0.4 to 0.7 μA and from 7.5 to 21 mW m^{-2} , respectively (see Figure 8h).^[149]

3.5. Electrode Modification

Apart from the triboelectric layer, the characteristics of the electrode layer, including material categories, structure, and shape, also significantly impact the output performance of TENGs. These factors influence the electrode layer's charge conduction capacity and the degree of contact with the triboelectric layer, subsequently affecting the overall output performance. In this section, instances are provided from two perspectives, rigid and flexible electrodes, showcasing strategies to enhance the output of TENG.

Rigid electrodes offer excellent stability, high stiffness, and outstanding conductivity. The output results can be effectively optimized when combined with specialized fabrication techniques and structural design. Due to the inherent characteristics of rigid materials, researchers often create patterned microstructures on the surface or design specific shapes for rigid electrodes to increase their contact area with the triboelectric layer for electrical output enhancement. Specifically, laser direct writing (LDW) is commonly adopted to create patterned electrode layers due to its powerful, precisely programmable, and mask-free fabrication process.^[150,151] Coupled with LDW technology, Zhu et al. fabricated a customizable patterned laser-induced Cu (LIC) electrode utilizing the metal Cu with excellent conductivity, high robust-

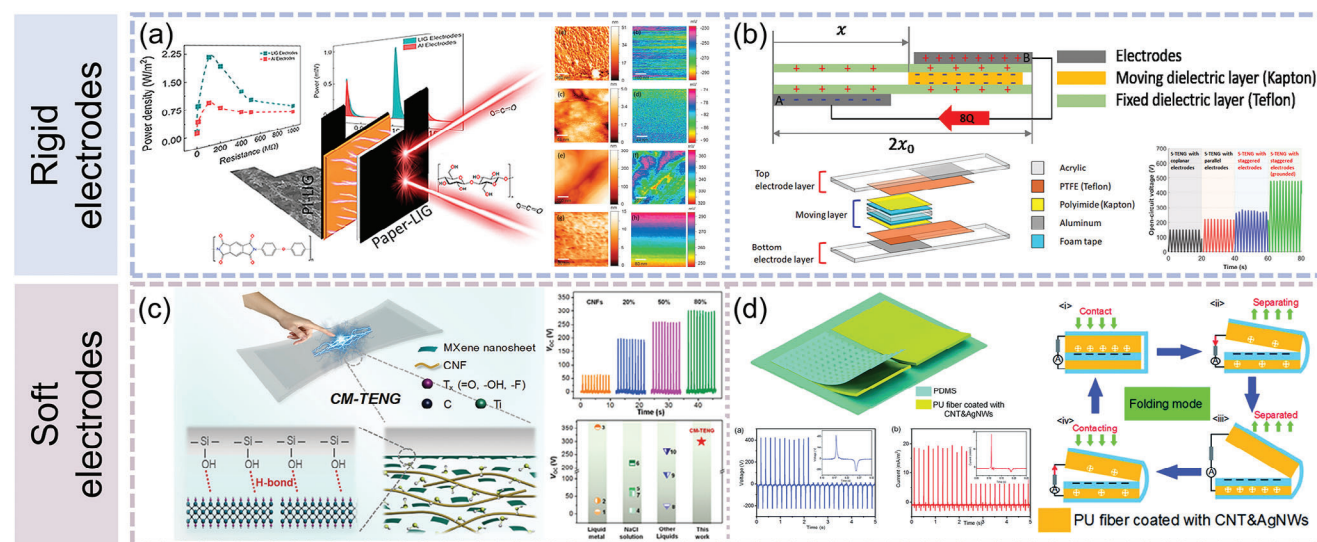


Figure 9. Electrodes modification. Rigid electrodes include a) a high crystallinity, sp^2 -hybridized laser-induced graphene (LIG) as the electrode using CO_2 laser direct writing. Reproduced with permission.^[153] Copyright 2020, Elsevier. b) A sliding-mode TENG with staggered electrodes (S-TENG-SE). Reproduced with permission.^[154] Copyright 2021, Elsevier. Soft electrodes include c) MXene-based composite dispersions as highly flexible liquid electrodes. Reproduced with permission.^[161] Copyright 2020, John Wiley and Sons/Wiley-VCH. d) A coplanar electrode using electrospun polyurethane (PU) nanofibers and conductive nanomaterials as stretchable electrodes. Reproduced with permission.^[162] Copyright 2017, Royal Society of Chemistry.

ness, and low cost as the thin-film electrode material, which held a high conductivity of $0.4 \Omega \text{ sq}^{-1}$, mechanical durability, and long-term stability. The fabricated LIC-based TENG ($30 \times 30 \text{ mm}^2$) with nylon film and P(VDF-TrFE) film as tribo-positive and tribo-negative materials, respectively, enables high output performances (a V_{oc} exceeding 200 V, an I_{sc} of $27.4 \mu\text{A}$, and a maximum instantaneous output power of 3.0 W m^{-2}).^[152] Furthermore, Zhao et al. reported a high crystallinity, sp^2 -hybridized laser-induced graphene (LIG) as a high-efficiency electrode for TENG. Using CO_2 laser direct writing, the surface of tribo-negative PI and tribo-positive cellulosic paper is converted into corresponding PI-LIG and paper-LIG, respectively. The LIG-based paper-PI TENG presents much higher electrical output characteristics with a peak-to-peak voltage of $\approx 625 \text{ V}$, current density of $\approx 20 \text{ mA m}^{-2}$, transfer charge density of $\approx 138 \mu\text{C m}^{-2}$, and maximum power output of $\approx 2.25 \text{ W m}^{-2}$, respectively. (The corresponding values of the conventional Al-tape electrode-based paper-PI TENGs are 400 V_{pp} , $\approx 10 \text{ mA m}^{-2}$, $\approx 85 \mu\text{C m}^{-2}$, and 0.9 W m^{-2} , respectively). This graphene electrode overcomes the drawbacks of poor bonding of the metal electrode to the soft polymer triboelectric layers and vulnerability to oxidation of liquid metal electrodes. It also exhibits high flexibility and an intimate electrical connection, remarkably increasing the output power of metal-free TENG by 150% (as shown in **Figure 9a**).^[153] Additionally, varying the spatial arrangement and shape of electrodes can yield favorable results. Lee et al. devised a sliding-mode TENG with staggered electrodes (S-TENG-SE), which enabled both the transfer charge and the V_{oc} to increase simultaneously due to the increased friction area and the reduced capacitance. Electrodes A and B are placed on different planes, and both sides experience friction when the dielectric layer moves. According to the principle of charge conservation, the SCD of the moving dielectric layer doubles because the surface area of the moving dielectric layer is half of the fixed dielectric layer. Moreover, by a grounded

shielding electrode in the moving dielectric layer (PI), the maximum V_{oc} , transfer charge, and I_{sc} of S-TENG-SE increased by 3.3, 2.7, and 4.5 times, respectively, compared to the conventional S-TENG with coplanar electrodes. This configuration facilitates superior output levels (**Figure 9b**).^[154] Moreover, a novel TENG integrated with a wave structure electrode (W-TENG) has been reported. Compared to the TENG with traditional flat plate electrodes, the W-TENG achieves higher output performance, with at least a two-fold increase in V_{oc} , I_{sc} , and transfer charge. The maximum instantaneous output power of 0.94 mW is obtained at 6 Hz. The reason for different electrical outputs of electrodes with various morphologies and structures lies in the capacitance between the electrode and the surface of triboelectric material, which determines the accumulation of triboelectric charge. In other words, the electrode layer with a larger surface area will accumulate more charges on the surface of triboelectric materials, thereby enhancing the output performance of the TENG device.^[155]

The development and application of shape-adaptive flexible electrode materials are also critical for high-output performance TENG, encompassing liquid electrodes, organic polymers, and ionic conductors. Recently, liquid electrodes with high electron mobility and super deformability, such as liquid metal,^[156,157] physiological saline,^[158,159] and GO dispersion,^[160] have been regarded as effective electron collectors that can be combined with flexible elastomers to construct SE-TENGs. For instance, 2D MXene is an attractive electrode material known for its remarkable electronic conductivity and negatively charged surface. Cao et al. used CNFs as a dispersant and interlocking agent to promote the interconnections between 2D MXene nanosheets. A stretchable and shape-adaptive CNF/MXene-TENG (CM-TENG) was demonstrated, in which MXene-based composite dispersions as highly flexible liquid electrodes. MXene nanosheets with higher electron affinity can render the integral triboelectric layer more

negative, injecting more electrons from the tribo-positive layer to the tribo-negative one. CM-TENG with an effective electrode area of $6.0 \times 2.5 \text{ cm}^2$ can generate a V_{oc} of $\approx 300 \text{ V}$, approximately five times higher than the TENG based on CNFs dispersion liquid-electrode, suggesting outstanding output performance (see Figure 9c).^[161] Additionally, Chen et al. developed an ultrathin stretchable TENG (s-TENG) with coplanar electrodes using electrospun polyurethane (PU) nanofibers and conductive nanomaterials as stretchable electrodes. The electrodes using stretchable PU nanofibers and conductive nanomaterials allow the s-TENG to maintain high conductivity ($< 250 \text{ } \Omega \text{ cm}^{-1}$) even after being stretched by 100%. Furthermore, the increased contact area between micro-structured PDMS and porous, non-woven structured nanofibers heightens the charge transfer capability of the coplanar double-electrode TENG. This device (with a contact area of $1.5 \times 3.5 \text{ cm}^2$) can generate a peak voltage of 670 V and a peak current density of 23.9 mA m^{-2} even in the folding/unfolding working situation, which surpasses those of previously reported stretchable SE-TENG (6 mA m^{-2}) and rubber-based TENG (1.35 mA m^{-2}) (Figure 9d).^[162] Moreover, flexible ionic conductors, such as conductive hydrogels, are alternative electrodes for stretchable and transparent TENGs, which transfer charge by ions within the polymer matrix.^[163] Jing et al. conducted the first verification of the distinct impact of hydrogel viscoelastic property on hydrogel-based TENG (H-TENG) and observed that the output voltage decreased with increasing stretch ratio. A hybrid double-network hydrogel electrode layer composed of polyvinyl alcohol and alginate was prepared, and the existence of ions greatly improved the conductivity of hydrogels. The optimum H-TENG exhibits stable and high output performance, with the peak output voltage and current reaching 203.4 V and $17.6 \text{ } \mu\text{A}$, respectively, and a power density of 0.98 W m^{-2} . Furthermore, the research also revealed that elastic H-TENG exhibited superior output performance than rigid one due to its elastic response when subjected to external force.^[164]

4. Challenges and Prospect

This review systematically introduces strategies to enhance the output performance of TENG from five key aspects: triboelectric material selection, surface modification, material component composition, device structure design, and electrode modification. The selection and modification of triboelectric layers and electrode materials offer straightforward, rapid, and effective advantages. Furthermore, the structural design of the overall device and functional layer not only bolsters the output performance but also expands the range of potential application scenarios, ultimately elevating the efficiency of mechanical energy harvesting.

Nevertheless, achieving widespread applications for high-output performance TENGs still encounters several challenges. First, at the theoretical level, further clarity and precision are required in the research on triboelectrification, charge generation, and charge transfer mechanisms. Second, balancing the enhancement of the output performance while maintaining and improving long-term stability, shape adaptability, environmental suitability, and miniaturization presents a challenge. The following aspects should be explored to further improve the output performance of TENG.

- 1) Theoretical research needs refinement. In-depth research is required to investigate the micro-mechanisms of CE and provide reliable theoretical support. The mechanism of triboelectrification is not yet fully understood. The quantitative matching between triboelectric microstructure and triboelectric charge generation remains a puzzle. The effect of the material's dielectric properties, work function, conductivity, and roughness on the output performance needs further quantitative analysis. Alongside experimental investigations, establishing accurate theoretical models will facilitate further advancements in the research, enabling the enhancement of the output performance.
- 2) The scope of material choices desires expansion. Suitable material selection is the first step to preparing high-output performance TENGs. As the application scenarios of TENG continue to expand, it is urgent to develop a wide range of materials to fabricate devices with excellent properties and meet practical application requirements. For instance, intelligent wearable electronic devices demand highly flexible and portable materials, while implantable electronic devices need materials with high biosafety and shape adaptability. Besides, transient electronic devices require a broader selection of biodegradable materials. The conductivity, flexibility, and stability of electrode materials are also of great significance to the output characteristics of TENG.
- 3) Device stability demands improvement. Compared to the controlled laboratory conditions, the actual operating environments are considerably more complex. This heightened complexity poses a challenge in maintaining long-term, stable, and high-output performance in these devices. Many existing materials with nanostructures are prone to wear and lack durability, which can result in damage or detachment during cyclic friction processes. To address this challenge, a practical strategy is to opt for robust triboelectric and electrode materials, ensuring the integrity of nanostructures over extended periods of operation. Additionally, incorporating external encapsulation layers serves as a protective barrier, isolating the core functional layers from external damaging factors like moisture and impurities. Future research endeavors should be dedicated to the design and development of TENG devices that not only exhibit long-term stability but also deliver high-output performance. This will enable their use in various applications, even under adverse conditions such as high temperatures, high humidity, and acidic or alkaline environments, promoting their widespread adoption.
- 4) Device miniaturization. The devices are expected to become more compact and lightweight, offering benefits such as cost reduction, energy conservation, and improved integration with artificial intelligence. Simultaneously, there is a pressing need to enhance the energy conversion efficiency of these devices. This is particularly crucial in applications related to human-oriented power supply, monitoring, sensing, and electrical stimulation, where the prevailing trend is geared toward miniaturization and low power consumption, enabling seamless integration with other electronic systems.

In summary, the advent of TENG has provided a new avenue for energy utilization, with notable advancements achieved in both theoretical and experimental research. Nevertheless,

improving the output performance of TENG is vital for its applications in various fields, including blue energy harvesting, self-driving sensors, self-powered wearable devices, electronic medical devices, and more. It is hoped that in the future, more efficient, reliable, practical, and cost-effective methods will be developed to optimize the output performance of TENG and promote its widespread adoption and integration into various aspects of human life.

Acknowledgements

This work was supported by the National Key Research and Development Program of China (2022YFB3804700, 2021YFB3200303), the National Natural Science Foundation of China (T2125003, 52203325), Beijing Natural Science Foundation (JQ20038, L212010), and the Fundamental Research Funds for the Central Universities (E0EG6802X2).

Conflict of Interest

The authors declare no conflict of interest.

Keywords

electrode modification, output performance, structural optimization, triboelectric materials, triboelectric nanogenerators

Received: December 4, 2023

Revised: January 22, 2024

Published online:

- [1] F.-R. Fan, Z.-Q. Tian, Z. L. Wang, *Nano Energy* **2012**, *1*, 328.
- [2] S. H. Wang, L. Lin, Z. L. Wang, *Nano Lett.* **2012**, *12*, 6339.
- [3] C. C. Shan, W. L. Liu, Z. Wang, X. J. Pu, W. C. He, Q. Tang, S. K. Fu, G. Li, L. Long, H. Y. Guo, J. F. Sun, A. P. Liu, C. G. Hu, *Energy Environ. Sci.* **2021**, *14*, 5395.
- [4] Z. L. Wang, *ACS Nano* **2013**, *7*, 9533.
- [5] T. H. Cheng, J. J. Shao, Z. L. Wang, *Nat. Rev. Methods Primers* **2023**, *3*, 39.
- [6] B. Chen, Y. Yang, Z. L. Wang, *Adv. Energy Mater.* **2018**, *8*, 1702649.
- [7] J. Bae, J. Lee, S. Kim, J. Ha, B. S. Lee, Y. Park, C. Choong, J. B. Kim, Z. L. Wang, H. Y. Kim, J. J. Park, U. I. Chung, *Nat. Commun.* **2014**, *5*, 4929.
- [8] Z. C. Quan, C. B. Han, T. Jiang, Z. L. Wang, *Adv. Energy Mater.* **2016**, *6*, 1501799.
- [9] A. Ahmed, *J. Mater. Chem. A* **2022**, *10*, 1992.
- [10] L. Xu, Y. K. Pang, C. Zhang, T. Jiang, X. Y. Chen, J. J. Luo, W. Tang, X. Cao, Z. L. Wang, *Nano Energy* **2017**, *31*, 351.
- [11] J. Chen, J. Yang, Z. L. Li, X. Fan, Y. L. Zi, Q. S. Jing, H. Y. Guo, Z. Wen, K. C. Pradel, S. M. Niu, Z. L. Wang, *ACS Nano* **2015**, *9*, 3324.
- [12] H. Ouyang, Z. Liu, N. Li, B. Shi, Y. Zou, F. Xie, Y. Ma, Z. Li, H. Li, Q. Zheng, X. Qu, Y. Fan, Z. L. Wang, H. Zhang, Z. Li, *Nat. Commun.* **2019**, *10*, 1821.
- [13] H. Ryu, H.-m. Park, M.-K. Kim, B. Kim, H. S. Myoung, T. Y. Kim, H.-J. Yoon, S. S. Kwak, J. Kim, T. H. Hwang, E.-K. Choi, S.-W. Kim, *Nat. Commun.* **2021**, *12*, 4374.
- [14] S. Wang, H. L. Tai, B. H. Liu, Z. H. Duan, Z. Yuan, H. Pan, Y. J. Su, G. Z. Xie, X. S. Du, Y. D. Jiang, *Nano Energy* **2019**, *58*, 312.
- [15] S. Wang, X. Mu, X. Wang, A. Y. Gu, Z. L. Wang, Y. Yang, *ACS Nano* **2015**, *9*, 9554.
- [16] B. S. Zhang, Y. J. Tang, R. R. Dai, H. Y. Wang, X. P. Sun, C. Qin, Z. F. Pan, E. J. Liang, Y. C. Mao, *Nano Energy* **2019**, *64*, 103953.
- [17] S. H. Wang, Y. N. Xie, S. M. Niu, L. Lin, Z. L. Wang, *Adv. Mater.* **2014**, *26*, 2818.
- [18] S. H. Wang, S. M. Niu, J. Yang, L. Lin, Z. L. Wang, *ACS Nano* **2014**, *8*, 12004.
- [19] C. B. Han, W. M. Du, C. Zhang, W. Tang, L. M. Zhang, Z. L. Wang, *Nano Energy* **2014**, *6*, 59.
- [20] L. Long, W. L. Liu, Z. Wang, W. C. He, G. Li, Q. Tang, H. Y. Guo, X. J. Pu, Y. K. Liu, C. G. Hu, *Nat. Commun.* **2021**, *12*, 4689.
- [21] F. Xing, Y. Jie, X. Cao, T. Li, N. Wang, *Nano Energy* **2017**, *42*, 138.
- [22] Y. M. Zeng, H. J. Xiang, N. Zheng, X. Cao, N. Wang, Z. L. Wang, *Nano Energy* **2022**, *91*, 106601.
- [23] Y. Zou, P. C. Tan, B. J. Shi, H. Ouyang, D. J. Jiang, Z. Liu, H. Li, M. Yu, C. Wang, X. C. Qu, L. M. Zhao, Y. B. Fan, Z. L. Wang, Z. Li, *Nat. Commun.* **2019**, *10*, 2695.
- [24] X. L. Tao, X. Y. Chen, Z. L. Wang, *Energy Environ. Sci.* **2023**, *16*, 3654.
- [25] F. Yi, Z. Zhang, Z. Kang, Q. L. Liao, Y. Zhang, *Adv. Funct. Mater.* **2019**, *29*, 1808849.
- [26] Y. S. Gai, Y. G. Jiang, Z. Li, *Nano Energy* **2023**, *116*, 108787.
- [27] W. T. Cao, H. Ouyang, W. Xin, S. Y. Chao, C. Ma, Z. Li, F. Chen, M. G. Ma, *Adv. Funct. Mater.* **2020**, *30*, 2004181.
- [28] A. A. Mathew, A. Chandrasekhar, S. Vivekanandan, *Nano Energy* **2021**, *80*, 105566.
- [29] C. G. Zhang, Y. J. Hao, J. Y. Yang, W. Su, H. K. Zhang, J. Wang, Z. L. Wang, X. H. Li, *Adv. Energy Mater.* **2023**, *13*, 2300387.
- [30] Y. T. Hao, X. M. Li, B. D. Chen, Z. Y. Zhu, *Front. Mar. Sci.* **2022**, *9*, 1038035.
- [31] Y. H. Xu, W. X. Yang, X. H. Lu, Y. F. Yang, J. P. Li, J. M. Wen, T. H. Cheng, Z. L. Wang, *ACS Nano* **2021**, *15*, 16368.
- [32] F. X. Sun, Y. S. Zhu, C. J. Jia, T. M. Zhao, L. Chu, Y. P. Mao, *J. Energy Chem.* **2023**, *79*, 477.
- [33] D. J. Yu, Z. Li, W. Q. Xie, D. S. Li, Z. Li, Y. S. Li, *Nano Energy* **2022**, *103*, 107762.
- [34] Z. Li, Q. Zheng, Z. L. Wang, Z. Li, *Research* **2020**, *2020*, 8710686.
- [35] B. J. Shi, Z. Liu, Q. Zheng, J. P. Meng, H. Ouyang, Y. Zou, D. J. Jiang, X. C. Qu, M. Yu, L. M. Zhao, Y. B. Fan, Z. L. Wang, Z. Li, *ACS Nano* **2019**, *13*, 6017.
- [36] Y. Q. Yang, X. G. Guo, M. L. Zhu, Z. D. Sun, Z. X. Zhang, T. Y. Y. He, C. K. Lee, *Adv. Energy Mater.* **2023**, *13*, 2203040.
- [37] Z. Liu, H. Li, B. J. Shi, Y. B. Fan, Z. L. Wang, Z. Li, *Adv. Funct. Mater.* **2019**, *29*, 1808820.
- [38] Y. Wang, B. Li, T. Tian, Y. Liu, J. Zhang, K. Qian, *Trends Analyt. Chem.* **2022**, *149*, 116565.
- [39] W. J. Li, Y. T. Pei, C. Zhang, A. G. P. Kottapalli, *Nano Energy* **2021**, *84*, 105865.
- [40] J. D. Zou, M. Zhang, J. R. Huang, J. Bian, Y. Jie, M. Willander, X. Cao, N. Wang, Z. L. Wang, *Adv. Energy Mater.* **2018**, *8*, 1702671.
- [41] H. Y. Yum, S. A. Han, K. Konstantinov, S. W. Kim, J. H. Kim, *Adv. Mater. Technol.* **2023**, *8*, 2201500.
- [42] X. L. Ji, T. K. Zhao, X. Zhao, X. F. Lu, T. H. Li, *Adv. Mater. Technol.* **2020**, *5*, 1900921.
- [43] Z. Y. Che, S. O'Donovan, X. Xiao, X. Wan, G. R. Chen, X. Zhao, Y. H. Zhou, J. Y. Yin, J. Chen, *Small* **2023**, *19*, 2207600.
- [44] S. Parandeh, N. Etemadi, M. Kharaziha, G. R. Chen, A. Nashalian, X. Xiao, J. Chen, *Adv. Funct. Mater.* **2021**, *31*, 2105169.
- [45] D. J. Jiang, B. J. Shi, H. Ouyang, Y. B. Fan, Z. L. Wang, Z. Li, *ACS Nano* **2020**, *14*, 6436.
- [46] J. Zhu, T. Ding, K. Jin, Y. Xing, J. Huang, D. Xia, K. Cai, J. Zhang, *View* **2022**, *3*, 20220051.
- [47] J. Y. Shen, B. Li, Y. Y. Yang, Z. Yang, X. Liu, K. C. Lim, J. Q. Chen, L. H. Ji, Z. H. Lin, J. Cheng, *Biosens. Bioelectron.* **2022**, *216*, 114595.
- [48] S. N. Cui, L. L. Zhou, D. Liu, S. X. Li, L. Liu, S. Y. Chen, Z. H. Zhao, W. Yuan, Z. L. Wang, *J. Wang, Matter* **2022**, *5*, 180.

- [49] J. Wang, C. S. Wu, Y. J. Dai, Z. H. Zhao, A. Wang, T. J. Zhang, Z. L. Wang, *Nat. Commun.* **2017**, *8*, 88.
- [50] L. Cheng, Q. Xu, Y. B. Zheng, X. F. Jia, Y. Qin, *Nat. Commun.* **2018**, *9*, 3773.
- [51] S. H. Wang, Y. N. Xie, S. M. Niu, L. Lin, C. Liu, Y. S. Zhou, Z. L. Wang, *Adv. Mater.* **2014**, *26*, 6720.
- [52] R. Y. Zhang, H. Olin, *Ecomat.* **2020**, *2*, e12062.
- [53] G. Khandelwal, N. P. M. J. Raj, S. J. Kim, *Adv. Energy Mater.* **2021**, *11*, 2101170.
- [54] F. R. Fan, J. J. Luo, W. Tang, C. Y. Li, C. P. Zhang, Z. Q. Tian, Z. L. Wang, *J. Mater. Chem. A* **2014**, *2*, 13219.
- [55] Y. Lyu, Y. Wang, *Nano Energy* **2022**, *103*, 107811.
- [56] D. Kim, I. W. Tcho, I. K. Jin, S. J. Park, S. B. Jeon, W. G. Kim, H. S. Cho, H. S. Lee, S. C. Jeoung, Y. K. Choi, *Nano Energy* **2017**, *35*, 379.
- [57] W. G. Kim, D. W. Kim, I. W. Tcho, J. K. Kim, M. S. Kim, Y. K. Choi, *ACS Nano* **2021**, *15*, 258.
- [58] N. Y. Cui, L. Gu, Y. M. Lei, J. M. Liu, Y. Qin, X. H. Ma, Y. Hao, Z. L. Wang, *ACS Nano* **2016**, *10*, 6131.
- [59] B. L. Cheng, Q. Xu, Y. Q. Ding, S. Bai, X. F. Jia, Y. D. C. Yu, J. Wen, Y. Qin, *Nat. Commun.* **2021**, *12*, 4782.
- [60] C. X. Lu, C. B. Han, G. Q. Gu, J. Chen, Z. W. Yang, T. Jiang, C. He, Z. L. Wang, *Adv. Eng. Mater.* **2017**, *19*, 1700275.
- [61] V. Nguyen, R. S. Yang, *Nano Energy* **2013**, *2*, 604.
- [62] Y. Q. Hu, X. L. Wang, H. K. Li, H. Q. Li, Z. H. Li, *Nano Energy* **2020**, *71*, 104640.
- [63] W. Yang, J. Chen, G. Zhu, X. Wen, P. Bai, Y. Su, Y. Lin, Z. Wang, *Nano Res.* **2013**, *6*, 880.
- [64] S. M. Niu, Y. Liu, S. H. Wang, L. Lin, Y. S. Zhou, Y. F. Hu, Z. L. Wang, *Adv. Mater.* **2013**, *25*, 6184.
- [65] H. Yi, L. Xiong, *J. Comput. Electron.* **2020**, *19*, 1670.
- [66] H. Zhang, L. J. Yao, L. W. Quan, X. L. Zheng, *Nanotechnol. Rev.* **2020**, *9*, 610.
- [67] Y. H. Li, G. Z. Li, P. L. Zhang, H. D. Zhang, C. Ren, X. Shi, H. Cai, Y. X. Zhang, Y. S. Wang, Z. F. Guo, H. F. Li, G. F. Ding, H. G. Cai, Z. Q. Yang, C. Zhang, Z. L. Wang, *Adv. Energy Mater.* **2021**, *11*, 2003921.
- [68] D. Zhu, X. Guo, H. Y. Li, Z. T. Yuan, X. S. Zhang, T. H. Cheng, *Nano Energy* **2023**, *108*, 108233.
- [69] Y. J. Zou, J. Xu, K. Chen, J. Chen, *Adv. Mater. Technol.* **2021**, *6*, 2000916.
- [70] Y. H. Liu, Q. Fu, J. L. Mo, Y. X. Lu, C. C. Cai, B. Luo, S. X. Nie, *Nano Energy* **2021**, *89*, 106369.
- [71] X. Suo, B. Li, H. F. Ji, S. L. Mei, S. Miao, M. W. Gu, Y. Z. Yang, D. S. Jiang, S. J. Cui, L. G. Chen, G. Y. Chen, Z. Wen, H. B. Huang, *Nano Energy* **2023**, *114*, 108651.
- [72] V. A. Cao, S. Lee, M. Kim, M. M. Alam, P. Park, J. Nah, *Nano Energy* **2020**, *67*, 104300.
- [73] S. M. Niu, S. H. Wang, Y. Liu, Y. S. Zhou, L. Lin, Y. F. Hu, K. C. Pradel, Z. L. Wang, *Energy Environ. Sci.* **2014**, *7*, 2339.
- [74] D. Deepak, N. Soin, S. S. Roy, *Mater. Today Commun.* **2023**, *34*, 105412.
- [75] Z. T. Chen, K. R. Dai, J. X. Chen, J. T. Zhuo, D. N. Zhao, R. Ma, X. J. Zhang, X. B. Li, X. F. Wang, G. W. Yang, F. Yi, *Adv. Sci.* **2023**, *10*, 2206950.
- [76] C. Xu, A. C. Wang, H. Y. Zou, B. B. Zhang, C. L. Zhang, Y. L. Zi, L. Pan, P. H. Wang, P. Z. Feng, Z. Q. Lin, Z. L. Wang, *Adv. Mater.* **2018**, *30*, 1803968.
- [77] L. L. Zhou, Y. K. Gao, D. Liu, L. Liu, Z. H. Zhao, S. X. Li, W. Yuan, S. N. Cui, Z. L. Wang, J. Wang, *Adv. Energy Mater.* **2021**, 2101958.
- [78] Z. L. Wang, A. C. Wang, *Mater. Today* **2019**, *30*, 34.
- [79] H. M. Chen, S. J. Guo, S. C. Zhang, Y. Xiao, W. Yang, Z. Y. Sun, X. Cai, R. Fang, H. N. Wang, Y. Xu, J. Wang, Z. Li, *Energy Environ. Mater.* **2023**, *0*, e12654.
- [80] Y. Shi, H. R. Li, X. P. Fu, R. F. Luan, Y. X. Wang, N. Wang, Z. B. Sun, Y. X. Niu, C. H. Wang, C. Zhang, Z. L. Wang, *Nano Energy* **2023**, *110*, 108339.
- [81] S. W. Chen, X. Cao, N. Wang, L. Ma, H. R. Zhu, M. Willander, Y. Jie, Z. L. Wang, *Adv. Energy Mater.* **2017**, *7*, 1601255.
- [82] C. M. Cui, X. Z. Wang, Z. R. Yi, B. Yang, X. L. Wang, X. Chen, J. Q. Liu, C. S. Yang, *ACS Appl. Mater. Interfaces* **2018**, *10*, 3652.
- [83] S. M. Niu, Y. Liu, X. Y. Chen, S. H. Wang, Y. S. Zhou, L. Lin, Y. N. Xie, Z. L. Wang, *Nano Energy* **2015**, *12*, 760.
- [84] T. Jiang, W. Tang, X. Y. Chen, C. B. Han, L. Lin, Y. L. Zi, Z. L. Wang, *Adv. Mater. Technol.* **2016**, *1*, 1600017.
- [85] Y. X. Duan, H. X. Xu, S. J. Liu, P. F. Chen, X. Y. Wang, L. Xu, T. Jiang, Z. L. Wang, *Nano Res.* **2023**, *16*, 11646.
- [86] Y. Wang, Y. Yang, Z. L. Wang, *npj Flexible Electron.* **2017**, *1*, 10.
- [87] S. M. Niu, S. H. Wang, L. Lin, Y. Liu, Y. S. Zhou, Y. F. Hu, Z. L. Wang, *Energy Environ. Sci.* **2013**, *6*, 3576.
- [88] Y. K. Liu, W. L. Liu, Z. Wang, W. C. He, Q. Tang, Y. Xi, X. Wang, H. Y. Guo, C. G. Hu, *Nat. Commun.* **2020**, *11*, 1599.
- [89] J. Y. Zhang, Y. K. Gao, D. Liu, J. S. Zhao, J. Wang, *Nat. Commun.* **2023**, *14*, 3218.
- [90] L. Zhang, J. Hou, X. Bi, *J. Loss Prev. Process Ind.* **2013**, *26*, 1328.
- [91] Z. H. Zhao, J. Y. Zhang, W. Y. Qiao, L. L. Zhou, Z. T. Guo, X. Y. Li, Z. L. Wang, J. Wang, *Mater. Horiz.* **2023**, *10*, 5962.
- [92] J. Wen, H. He, C. Niu, M. Rong, Y. Huang, Y. Wu, *Nano Energy* **2022**, *96*, 107070.
- [93] G. B. Min, Y. Xu, P. Cochran, N. Gadegaard, D. M. Mulvihill, R. Dahiya, *Nano Energy* **2021**, *83*, 105829.
- [94] S. M. Niu, Z. L. Wang, *Nano Energy* **2015**, *14*, 161.
- [95] A. Chandrasekhar, V. Vivekananthan, G. Khandelwal, S. J. Kim, *Nano Energy* **2019**, *60*, 850.
- [96] Y. Sun, Y. D. Zheng, R. Wang, T. D. Lei, J. Liu, J. Fan, W. Shou, Y. Liu, *Nano Energy* **2022**, *100*, 107506.
- [97] Y. L. Zi, S. M. Niu, J. Wang, Z. Wen, W. Tang, Z. L. Wang, *Nat. Commun.* **2015**, *6*, 8376.
- [98] M. Seol, S. Kim, Y. Cho, K.-E. Byun, H. Kim, J. Kim, S. K. Kim, S.-W. Kim, H.-J. Shin, S. Park, *Adv. Mater.* **2018**, *30*, 1801210.
- [99] H. Y. Zou, L. T. Guo, H. Xue, Y. Zhang, X. F. Shen, X. T. Liu, P. H. Wang, X. He, G. Z. Dai, P. Jiang, H. W. Zheng, B. B. Zhang, C. Xu, Z. L. Wang, *Nat. Commun.* **2020**, *11*, 2093.
- [100] H. Y. Zou, Y. Zhang, L. T. Guo, P. H. Wang, X. He, G. Z. Dai, H. W. Zheng, C. Y. Chen, A. C. Wang, C. Xu, Z. L. Wang, *Nat. Commun.* **2019**, *10*, 1427.
- [101] M. Kim, S. H. Kim, M. U. Park, C. Lee, M. Kim, Y. Yi, K.-H. Yoo, *Nano Energy* **2019**, *65*, 104079.
- [102] R. Z. Pan, W. P. Xuan, J. K. Chen, S. R. Dong, H. Jin, X. Z. Wang, H. L. Li, J. K. Luo, *Nano Energy* **2018**, *45*, 193.
- [103] X. M. Wang, W. S. Tong, Y. N. Li, Z. H. Wang, Y. Y. Chen, X. Zhang, X. Wang, Y. H. Zhang, *Appl. Clay Sci.* **2021**, *215*, 106330.
- [104] X. Xia, Z. Q. Zhou, Y. H. Shang, Y. Yang, Y. L. Zi, *Nat. Commun.* **2023**, *14*, 1023.
- [105] N. Wang, H. Huang, W. X. Zhu, X. Zhao, Y. Yang, *Energy Technol.* **2022**, *10*, 2101156.
- [106] S. Parandeh, M. Kharaziha, F. Karimzadeh, *Nano Energy* **2019**, *59*, 412.
- [107] J. Qian, J. He, S. Qian, J. Zhang, X. Niu, X. Fan, C. Wang, X. Hou, J. Mu, W. Geng, X. Chou, *Adv. Funct. Mater.* **2020**, *30*, 1907414.
- [108] P. Ding, J. K. Chen, U. Farooq, P. F. Zhao, N. Soin, L. Y. Yu, H. Jin, X. Z. Wang, S. R. Dong, J. K. Luo, *Nano Energy* **2018**, *46*, 63.
- [109] J. C. Qian, J. He, S. Qian, J. Zhang, X. S. Niu, X. M. Fan, C. Wang, X. J. Hou, J. L. Mu, W. P. Geng, X. J. Chou, *Adv. Funct. Mater.* **2020**, *30*, 1907414.
- [110] Y. Y. Gao, B. A. Xu, D. Tan, M. Q. Li, Y. T. Wang, Y. J. Yang, *Chem. Eng. J.* **2023**, *466*, 143079.

- [111] Z. Zhang, Y. Y. Xu, D. F. Wang, H. G. Yang, J. S. Guo, L. S. Turng, *Nano Energy*. **2019**, *60*, 903.
- [112] Y. Yang, H. L. Zhang, R. Y. Liu, X. N. Wen, T. C. Hou, Z. L. Wang, *Adv. Energy Mater.* **2013**, *3*, 1563.
- [113] C. H. Yao, A. Hernandez, Y. H. Yu, Z. Y. Cai, X. D. Wang, *Nano Energy*. **2016**, *30*, 103.
- [114] Z. X. Zhang, J. Cai, *Curr. Appl. Phys.* **2021**, *22*, 1.
- [115] R. Ouyang, Y. Huang, H. T. Ye, Z. J. Zhang, H. Xue, *Nano Energy*. **2022**, *102*, 107749.
- [116] C. Z. Li, H. R. Zhang, Y. F. Wang, X. Y. Liu, A. Ali, Z. Q. Tian, *Adv. Mater. Technol.* **2023**, *8*, 2201791.
- [117] C. Rodrigues, M. Kumar, M. P. Proenca, J. Gutierrez, R. Melo, A. Pereira, J. Ventura, *Nano Energy*. **2020**, *72*, 104682.
- [118] S. Li, J. Nie, Y. Shi, X. Tao, F. Wang, J. Tian, S. Lin, X. Chen, Z. L. Wang, *Adv. Mater.* **2020**, *32*, 2001307.
- [119] H. Meng, Q. Yu, Z. Liu, Y. Gai, J. Xue, Y. Bai, X. Qu, P. Tan, D. Luo, W. Huang, K. Nie, W. Bai, Z. Hou, R. Tang, H. Xu, Y. Zhang, Q. Cai, X. Yang, Z. L. Wang, Z. Li, *Matter*. **2023**, *6*, 4274.
- [120] G. Du, J. Wang, Y. Liu, J. Yuan, T. Liu, C. Cai, B. Luo, S. Zhu, Z. Wei, S. Wang, S. Nie, *Adv. Sci.* **2023**, *10*, 2206243.
- [121] Y. Nurmakanov, G. Kalimulina, G. Naurzybayev, D. Adair, Z. Bakenov, *Nanoscale Res. Lett.* **2021**, *16*, 122.
- [122] S. Y. Li, Y. Fan, H. Q. Chen, J. H. Nie, Y. X. Liang, X. L. Tao, J. Zhang, X. Y. Chen, E. G. Fu, Z. L. Wang, *Energy Environ. Sci.* **2020**, *13*, 896.
- [123] Y. Fan, S. Y. Li, X. L. Tao, Y. F. Wang, Z. Q. Liu, H. Q. Chen, Z. F. Wu, J. Zhang, F. Ren, X. Y. Chen, E. G. Fu, *Nano Energy*. **2021**, *90*, 106574.
- [124] T. Prada, V. Harnchana, A. Lakhonchai, A. Chingsungnoen, P. Poolcharuansin, N. Chanlek, A. Klamchuen, P. Thongbai, V. Amornkitbamrung, *Nano Res.* **2022**, *15*, 272.
- [125] X. Ma, S. Y. Li, S. J. Dong, J. H. Nie, M. Iwamoto, S. Q. Lin, L. Zheng, X. Y. Chen, *Nano Energy*. **2019**, *66*, 104090.
- [126] S. Mishra, P. Supraja, D. Haranath, R. R. Kumar, S. Pola, *Nano Energy*. **2022**, *104*, 107964.
- [127] S. Jang, H. Kim, Y. Kim, B. J. Kang, J. H. Oh, *Appl. Phys. Lett.* **2016**, *108*, 143901.
- [128] J.-H. Zhang, Y. Li, J. Du, X. Hao, H. Huang, *J. Mater. Chem. A*. **2019**, *7*, 11724.
- [129] J. Li, M. Zhang, G. Ni, H.-Y. Mi, B. Dong, C. Liu, C. Shen, *J. Appl. Polym. Sci.* **2023**, *140*, e53351.
- [130] X. J. Li, C. M. Jiang, F. N. Zhao, L. Y. Lan, Y. Yao, Y. H. Yu, J. F. Ping, Y. B. Ying, *Nano Energy*. **2019**, *61*, 78.
- [131] A. Haleem, Z. Haider, R. U. S. Ahmad, U. P. Claver, A. F. Shah, G. Zhao, W. D. He, *Int. J. Energy Res.* **2020**, *44*, 8442.
- [132] P.-C. Lee, Y.-C. Ou, R.-C. Wang, C.-P. Liu, *Nano Energy*. **2021**, *89*, 106394.
- [133] H. Y. Meng, J. P. Wan, J. Y. Jing, D. Y. Sun, B. Y. Jiang, F. X. Liang, Z. Z. Yang, *Chin. Chem. Lett.* **2020**, *31*, 253.
- [134] H. Y. Meng, C. D. Zhang, Y. S. Gai, Q. Yu, Z. Li, *Compos. Part A Appl. Sci. Manuf.* **2022**, *159*, 106999.
- [135] M. Z. Y. Arkan, Z. Kinas, E. Arkan, C. O. Gökçe, K. Kara, A. Karabiber, M. Kus, F. Özel, *Int. J. Energy Res.* **2022**, *46*, 23517.
- [136] X. D. Yang, P. Li, B. Wu, H. W. Li, G. D. Zhou, *Curr. Appl. Phys.* **2021**, *32*, 50.
- [137] C. Wu, T. W. Kim, H. Y. Choi, *Nano Energy*. **2017**, *32*, 542.
- [138] L. K. Wang, H. C. Xu, F. C. Huang, X. M. Tao, Y. F. Ouyang, Y. L. Zhou, X. M. Mo, *Nanomaterials*. **2022**, *12*, 3217.
- [139] J. Zhang, Y. Zheng, L. Xu, D. Wang, *Nano Energy*. **2020**, *69*, 104435.
- [140] H. W. Liu, J. Dong, H. Y. Zhou, X. D. Yang, C. Y. Xu, Y. Q. Yao, G. D. Zhou, S. Zhang, Q. L. Song, *ACS Appl. Electron Mater.* **2021**, *3*, 4162.
- [141] M. H. Lai, B. L. Du, H. Y. Guo, Y. Xi, H. K. Yang, C. G. Hu, J. Wang, Z. L. Wang, *ACS Appl. Mater. Interfaces*. **2018**, *10*, 2158.
- [142] N. Y. Cui, J. M. Liu, Y. M. Lei, L. Gu, Q. Xu, S. H. Liu, Y. Qin, *ACS Appl. Energy Mater.* **2018**, *1*, 2891.
- [143] S. Y. Gao, Y. Chen, J. Z. Su, M. Wang, X. J. Wei, T. Jiang, Z. L. Wang, *ACS Nano*. **2017**, *11*, 3965.
- [144] S. A. Han, K. H. Lee, T. H. Kim, W. Seung, S. K. Lee, S. Choi, B. Kumar, R. Bhatia, H. J. Shin, W. J. Lee, S. Kim, H. S. Kim, J. Y. Choi, S. W. Kim, *Nano Energy*. **2015**, *12*, 556.
- [145] J. S. Chun, B. U. Ye, J. W. Lee, D. Choi, C. Y. Kang, S. W. Kim, Z. L. Wang, J. M. Baik, *Nat. Commun.* **2016**, *7*, 12985.
- [146] H. Feng, Y. Bai, L. Qiao, Z. Li, E. Wang, S. Chao, X. Qu, Y. Cao, Z. Liu, X. Han, R. Luo, Y. Shan, Z. Li, *Small*. **2021**, *17*, 2101430.
- [147] W. Du, X. Han, L. Lin, M. Chen, X. Li, C. Pan, Z. L. Wang, *Adv. Energy Mater.* **2014**, *4*, 1301592.
- [148] J. Fu, K. Xia, Z. Xu, *Sens. Actuator A Phys.* **2021**, *323*, 112650.
- [149] H. Lin, Y. Liu, S. Chen, Q. Xu, S. Wang, T. Hu, P. Pan, Y. Wang, Y. Zhang, N. Li, Y. Li, Y. Ma, Y. Xie, L. Wang, *Nano Energy*. **2019**, *65*, 103944.
- [150] X. N. Zang, C. Y. Jian, T. S. Zhu, Z. Fan, W. L. Wang, M. S. Wei, B. X. Li, M. F. Diaz, P. Ashby, Z. M. Lu, Y. Chu, Z. Z. Wang, X. R. Ding, Y. X. Xie, J. H. Chen, J. N. Hohman, M. Sanghadasa, J. C. Grossman, L. W. Lin, *Nat. Commun.* **2019**, *10*, 3112.
- [151] A. Chhetry, S. Sharma, S. C. Barman, H. Yoon, S. Ko, C. Park, S. Yoon, H. Kim, J. Y. Park, *Adv. Funct. Mater.* **2021**, *31*, 2007661.
- [152] S. L. Zhu, Y. F. Xia, Y. Zhu, M. Wu, C. Y. Jia, X. Wang, *Nano Energy*. **2022**, *96*, 107116.
- [153] P. Zhao, G. Bhattacharya, S. J. Fishlock, J. G. M. Guy, A. Kumar, C. Tsonos, Z. Yu, S. Raj, J. A. McLaughlin, J. Luo, N. Soin, *Nano Energy*. **2020**, *75*, 104958.
- [154] Y. Lee, S. G. Kang, J. Jeong, *Nano Energy*. **2021**, *86*, 106062.
- [155] Y. Qin, *Curr. Appl. Phys.* **2022**, *39*, 122.
- [156] S. Wang, L. Ding, X. W. Fan, W. Q. Jiang, X. L. Gong, *Nano Energy*. **2018**, *53*, 863.
- [157] Y. Q. Yang, N. Sun, Z. Wen, P. Cheng, H. C. Zheng, H. Y. Shao, Y. J. Xia, C. Chen, H. W. Lan, X. K. Xie, C. J. Zhou, J. Zhong, X. H. Sun, S. T. Lee, *ACS Nano*. **2018**, *12*, 2027.
- [158] F. Yi, X. F. Wang, S. M. Niu, S. M. Li, Y. J. Yin, K. R. Dai, G. J. Zhang, L. Lin, Z. Wen, H. Y. Guo, J. Wang, M. H. Yeh, Y. L. Zi, Q. L. Liao, Z. You, Y. Zhang, Z. L. Wang, *Sci. Adv.* **2016**, *2*, e150162.
- [159] X. F. Wang, Y. J. Yin, F. Yi, K. R. Dai, S. M. Niu, Y. Z. Han, Y. Zhang, Z. You, *Nano Energy*. **2017**, *39*, 429.
- [160] Y. H. Wu, Y. Luo, J. K. Qu, W. A. Daoud, T. Qi, *Nano Energy*. **2019**, *64*, 103948.
- [161] W.-T. Cao, H. Ouyang, W. Xin, S. Chao, C. Ma, Z. Li, F. Chen, M.-G. Ma, *Adv. Funct. Mater.* **2020**, *30*, 2004181.
- [162] X. X. Chen, Y. Song, H. T. Chen, J. X. Zhang, H. X. Zhang, *J. Mater. Chem. A*. **2017**, *5*, 12361.
- [163] T. Liu, M. M. Liu, S. Dou, J. M. Sun, Z. F. Cong, C. Y. Jiang, C. H. Du, X. Pu, W. G. Hu, Z. L. Wang, *ACS Nano*. **2018**, *12*, 2818.
- [164] X. Jing, H. Li, H. Y. Mi, P. Y. Feng, X. M. Tao, Y. J. Liu, C. T. Liu, C. Y. Shen, *ACS Appl. Mater. Interfaces*. **2020**, *12*, 23474.



Cong Li received her Bachelor's degree from the Civil Aviation University of China in 2021. Now, she is currently studying for a Master's degree as a joint student under the supervision of Professor Zhou Li at the Beijing Institute of Nanoenergy and Nanosystems, Chinese Academy of Sciences, Beijing, China. Her research focuses on biodegradable materials.



Yuan Bai received his Bachelor's degree from the College of Chemistry, Chongqing Normal University in 2018. Now, he is pursuing a Ph.D. degree at the School of Physical Science and Engineering Technology, Guangxi University. He is currently a joint student at Beijing Institute of Nanoenergy and Nanosystems, Chinese Academy of Science. His research interests are high-voltage TENG and piezoelectric materials.



Jiajia Shao received his Ph.D. degree from the University of Chinese Academy of Sciences (UCAS) in 2019, under the supervision of Prof. Zhonglin Wang. Since 2019, he has worked as a postdoctoral fellow (supervision: Prof. Zhong Lin Wang) at the Beijing Institute of Nanoenergy and Nanosystems (BINN), Chinese Academy of Sciences. He is now a researcher/professor at BINN, and the School of Nanoscience and Technology, UCAS. His research interests have been focused on the field of Maxwell's equations and displacement current, triboelectric nanogenerators, and physical mechanisms of contact electrification, modeling, and simulation of dynamic physical systems.



Hongyu Meng obtained his Ph.D. from the Institute of Chemistry, Chinese Academy of Sciences in 2019. Presently, he is an assistant professor at Beijing Institute of Nanoenergy and Nanosystems, Chinese Academy of Sciences. His research focuses on bio-composite materials and biodegradable electronic devices.



Zhou Li received his Ph.D. from Peking University in the Department of Biomedical Engineering in 2010 and a Bachelor's Degree from Wuhan University in 2004. He joined the School of Biological Science and Medical Engineering of Beihang University in 2010 as an associate professor. Currently, he is a professor at Beijing Institute of Nanoenergy and Nanosystems, Chinese Academy of Sciences. His research interests include nanogenerators, in vivo energy harvesters, self-powered medical devices, and biosensors.